



Contents lists available at ScienceDirect

Journal of Archaeological Science: Reports

journal homepage: www.elsevier.com/locate/jasrep

50,000 years of archaeological site stratigraphy and micromorphology in Boodie Cave, Barrow Island, Western Australia

I. Ward^{a,*}, P. Veth^a, L. Prossor^b, T. Denham^b, K. Ditchfield^a, T. Manne^d, P. Kendrick^e, C. Byrne^a, F. Hook^a, U. Troitzsch^c^a School of Social Sciences, M257, University of Western Australia, Crawley, WA 6009, Australia^b School of Archaeology and Anthropology, Australian National University, Canberra, ACT 2601, Australia^c Research School of Earth Sciences, Australian National University, Canberra, ACT 2601, Australia^d School of Social Science, The University of Queensland, Brisbane, QLD 4072, Australia^e Department of Parks and Wildlife, Locked Bag 104, Bentley Delivery Centre, WA 6983, Australia

A B S T R A C T

This study explores the application of soil micromorphological and automated scanning electron microscopy mineralogical analysis to characterise lithological boundaries and site formation history from an archaeological cave site on Barrow Island, northwestern Australia. The high-resolution characterisation is used to document the changing depositional context within Boodie Cave from the earliest period of occupation around 50 ky BP through to when transgressing seas isolated the island around 7 ky BP. Comparisons are made between excavations at the front of the cave — where stratigraphic integrity is high and a thicker, more comprehensive early Holocene sequence is preserved, with excavations inside the cave — where stratigraphic integrity is lower but an older Pleistocene record is preserved. The combination of these depositional scenarios provides a complete stratigraphic sequence for Boodie Cave, with depositional contacts defined at macro-, meso- and micro-scale levels. These contacts include erosive surfaces and trampled (ground) surfaces, such as the upper interface of SU5 and SU4. Based on the mineralogical and textural variations (microfacies) preserved within each unit, the vertical mixing zone is estimated to be between 1 and 5 cm. This reworking has not affected the general sequence of sedimentological (including grain size and mineralogy) and macro-cultural changes, which record an increasingly marine-dominated assemblage as the coastline encroaches. The integration of microscopic observations with anthracological, archaeomalacological, zooarchaeological and lithic analyses provides a more dynamic and comprehensive dialogue for interpreting the formation history of Boodie Cave and likely other early occupation sites from northern Australia.

1. Introduction

Located approximately half-way to the edge of the continental shelf of Australia, Barrow Island (Fig. 1) is optimally located to register the changing coastal landscape from earliest phases of human occupation through the post-glacial transgression and subsequent islandisation in the early Holocene. Fundamental to understanding this changing cultural landscape are the sediments, which in addition to providing context for cultural finds, also record ongoing natural processes and abrupt events within the occupation sequences under investigation — here focused on Boodie Cave on the exposed NW side of Barrow Island (Fig. 1). Boodie Cave (~100 m long and 20 m wide) is the largest of some 20 caves and rockshelters on Barrow Island. Over 20 m³ of deposit was excavated from this cave over a 3 year period, and provides a

cultural record expanding back to 51.1–46.2 ky BP or earlier (Veth et al., 2014, 2017). Boodie Cave has already presented unique insights into the changing nature of Aboriginal occupation and coastal resource use in response to post-glacial sea-level rise (Manne and Veth, 2015). The stratigraphic and sedimentological context of Boodie Cave's archaeological record is therefore critical in establishing the integrity of the archaeological deposits and to aid in local palaeoenvironmental reconstructions.

This paper uses the explanatory power of micromorphology to interpret the complexities within and beyond the cave. It presents a summary of the stratigraphic and microstratigraphic analyses undertaken from excavations within Boodie Cave, with the aim of understanding the archaeological integrity of the deposit and formation history of the cave. Following Mallol and Mentzer (2015), particular focus

* Corresponding author.

E-mail address: ingrid.ward@uwa.edu.au (I. Ward).

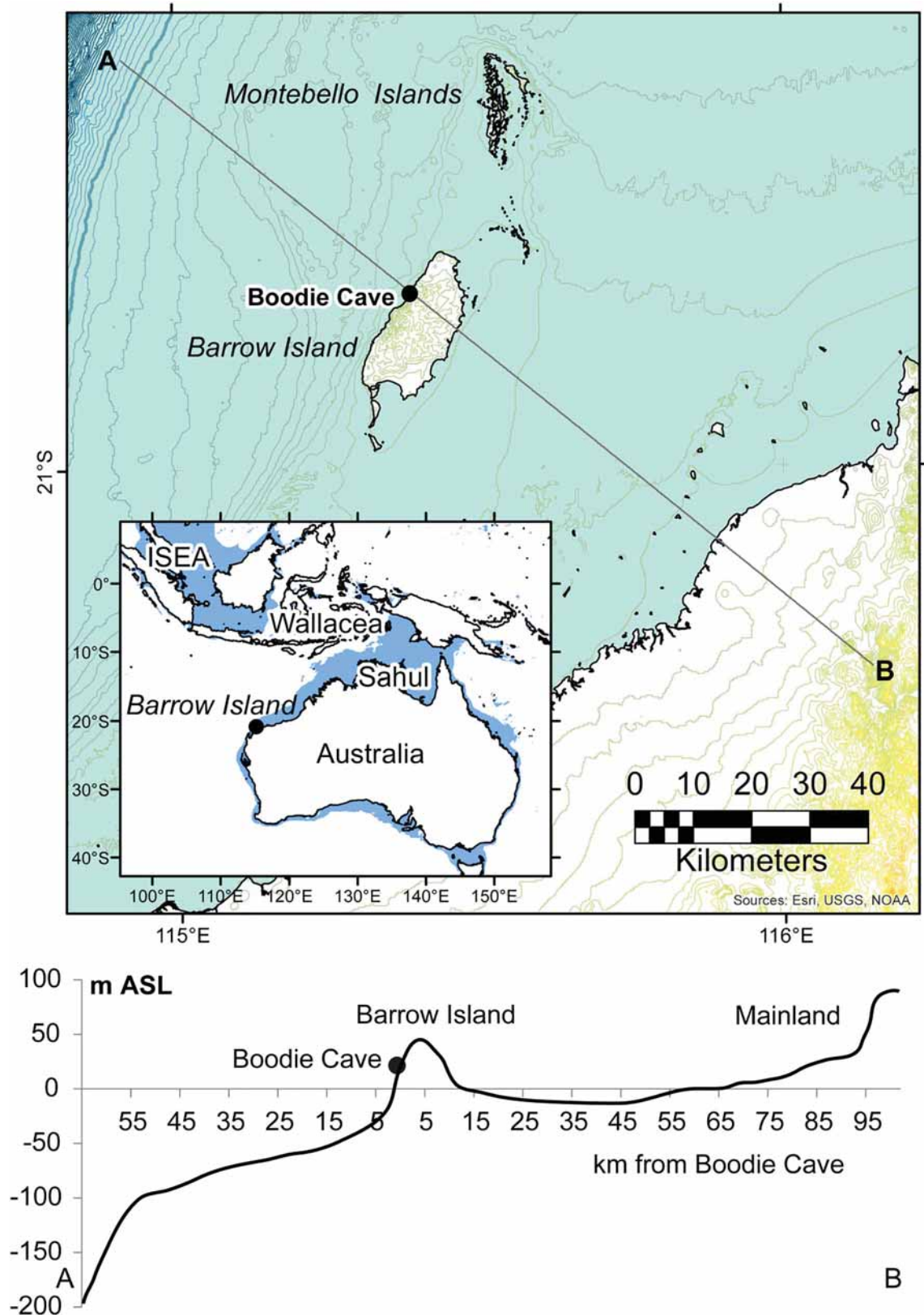


Fig. 1. Location map of Boodie Cave on continental shelf. (From Veth et al., 2017.)

is given to the nature of contacts and their significance for archaeological interpretation. In addition, automated petrographic analysis is used to provide bulk modal mineralogy and micron-scale compositional maps of sediments within the cave (Haberlah et al., 2011; see also Ward

et al., 2017). Despite the potential benefits of microstratigraphic approaches for obtaining a more accurate perception of time and context for the archaeological record (Courty et al., 1989), archaeological micromorphology remains an underutilised and nascent field (Goldberg



Fig. 2. Photo of Boodie Cave (circled) on the NW side of Barrow Is.
(Photo taken by IW.)

and Aldeias, 2016) and particularly so in Australia (Jankowski et al., 2015; Vanniewenhuyse et al., 2017). By integrating microscopic and mesoscopic data with anthracology, malacology, zooarchaeology and lithic analyses, this paper attempts to provide a more dynamic and comprehensive framework for interpreting the formation history of Boodie Cave and its changing environmental context.

1.1. Regional geomorphology and general location details

Barrow Island rises to 60 m asl and is separated from the Onslow coast by a 56 km shallow water (< 20 m) strait (Fig. 1). On the exposed western side of Barrow Island, the shelf edge steepens towards the continental shelf edge (Fig. 1). The island itself is composed almost entirely of Tertiary limestone outcrops, including Eocene Giralia calcarenite and mid- to late Miocene Trealla Limestone, the latter forming the major plateau surfaces and exposures in coastal cliffs (Hickman and Strong, 2003). Various Plio-Pleistocene calcarenite and aeolianite units are present around the margin, with high (< 30 m) sand dunes confined to the north side of the island. A general summary of the regional geomorphic and geoarchaeological context of the North West Shelf (NWS) region is provided by Ward et al. (2015).

On the western side of the island, where Boodie Cave is located (Fig. 2), the topography varies from rocky weathered 10–30 m high cliffs to less steep inclines, with narrow sandy beaches located between rocky headlands (Moro and Lagdon, 2013). Steep valleys with ephemeral drainage cut east-west into the escarpments and exposed limestone ridges supporting small pockets of *Eucalyptus* spp. (Moro and Lagdon, 2013). Large blocks (up to 5.2 × 2.5 × 2.0 m) of oyster-covered beachrock, thought to have been the products of mega-tsunamis, are found behind the coastal cliffs on Barrow Island. These have been dated to 5444–3498 years BP (Playford, 2014). Offshore intertidal limestone pavements lead out to low relief subtidal reef systems that form part of the Montebello/Barrow Island marine conservation reserves (DEC, 2007).

The central part of the island (reaching 62 m above sea level) is flatter with a skeletal (< 1 m) soil mantle and a low hummock-grass steppe dominated by *Triodia wiseana*. The eastern (leeward) side of the island has a slight gradient to the ocean, and is characterised by low rocky headlands, vegetated sand dunes and expansive nearshore intertidal and subtidal reefs, tidal flats and limited mangrove communities (Moro and Lagdon, 2013). Tides are semi-diurnal and moderate (3 m at MHWs), which combined with a shallow bathymetry along the

east side of the island, results in large areas of exposed seabed at low tide. Modelling indicates tidal range would have been as great, or greater, during the Last Glacial Maximum (LGM) resulting in even more expansive intertidal ecosystems for people to exploit (Ward et al., 2013).

A shallow unconfined aquifer on Barrow Island forms a lens of fresh to brackish groundwater at depths between 9 m and 53 m, floating upon denser, saline ground water located predominantly within the Tertiary Limestone (Chevron Australia, 2014). The freshwater lens extends across the island to within 200 to 500 m of the coast where tidal influences prevent the formation of a stable low salinity lens (Chevron Australia, 2014). Permanent surface water sources occur in freshwater seeps, and may have flowed out onto the extended shelf at times of lower sea level (Faure et al., 2002). These likely provided a critical resource for past occupants of the island until sea level rise rendered them brackish.

Prevailing winds are south to south-westerly (mean 6.6 m/s, max 16.2 m/s) during the summer months (October–March) and north-westerly to south-easterly (mean 5.8 m/s, max 19.4 m/s) during the winter months (April–September). Barrow Island is located in a region with very frequent Tropical Cyclone activity, with one cyclone every two years passing within 50 nautical miles of the island.¹ However, despite the extreme strength of some of these cyclones (with winds recorded at 408 km/h, BoM), few of these have significant effects beyond coastal inundation by storm surge, run-off inundation in low-lying parts of the island, and movement of sandy sediments in blowout areas. Located ~22 m above mean sea level, Boodie Cave is minimally impacted by any storms except under exceptional conditions (high tide, large surge, westerly winds, tsunami events; see Playford, 2014). In the 2014–2015 tropical cyclone season, Barrow Island was brushed by Cyclone Olwyn (Category 1), with wind gusts of 128 km/h and 141.6 mm of rain recorded on the island.² The main evidence of this cyclone in Boodie Cave was the development of a ~20 cm wide and shallow gully near the entrance, and small runoff channels towards the 2014 excavation (A106/A107); the latter were documented by Veth et al. (2014: Fig. 3B and C). Larger cyclones may result in greater erosion near the cave entrance.

Boodie Cave itself is a partially-closed calcarenite cave within the

¹ www.bom.gov.au/cyclone/history/wa/onslow.shtml.

² 'Barrow Island 24 Hour Observations'. Daily Observations. Weatherzone. 12 March 2015. Retrieved 22 March 2015.



Fig. 3. Photo of inside of Boodie Cave taken (A) in 2014 and (B) in 2015, after Cyclone Olwyn (Category 1). Arrows show direction of scouring and runoff into the cave.

Trealla Limestone formation, located 22 m above modern sea level on the western coast of Barrow Island. The cave is extensive, measuring approximately 100 m in length by up-to 20 m in width and has multiple chambers. The front of the west-facing cave, with a narrow vertical entry (roughly 7.7 m wide and 1–2 m high at the dripline), is now largely sheltered from the prevailing winds by *Ficus platypoda* bushes and fallen blocks of calcarenite. It is estimated that Boodie Cave has up to a thousand cubic metres of cultural deposits with the highest densities recorded near the seaward entrance.

2. Methods

2.1. Excavations — site plan, general stratigraphy and chronology

Sediments in the central zone of the cave have been reworked by Burrowing Bettong (*Bettongia lesueur*), hence all excavations were conducted in the ‘light zone’ nearer the main entrance (Fig. 3). This paper focuses on five 1 × 1 excavation trenches within Boodie Cave including A106 (2 m deep) and A102/A103 (1.8 m deep), situated ~6 m inside the cave, and E101/F101 (1.3 m deep) situated just inside the modern dripline (inset Fig. 4). These sequences provide a contrasting stratigraphic profile, with the sediments inside the cave

preserving a stratigraphically-indistinct but relatively expanded Pleistocene chronology and sediments near the entrance preserving a well-differentiated post-glacial and Holocene chronology (Veth et al., 2017). Nine major stratigraphic units (SUs) are identified, with SU4 – a dense midden unit – only present in the profiles at the front of the cave (Fig. 4C), and SU8 and SU9 only present inside the cave (Fig. 4B). The general chronological and archaeological context is summarised in Table 1, and detailed in full in Veth et al. (2017).

The sediments within Boodie Cave comprise both endogenous and exogenous inorganic material, as well as a significant contribution of cultural (bone, plant and lithic) material. Texturally the sediments comprise dry, loose, poorly to moderately sorted coarse, carbonate sands with abundant limestone fragments, grading into increasingly moist, moderately compacted, moderately-sorted silty sands. Towards the base, the sediments are coarse but more quartz-rich, before a relatively sharp transition to more clay-rich sediments at the very base. The sediments are uniformly alkaline (pH 8.5), helping to preserve the diverse and rich faunal assemblage (Manne and Veth, 2015). Bio-turbation is evident in the form of insect and small root channels (some unfilled), and fine rootlets particularly on the eastern wall of A103 (see Veth et al., 2017). Large roots were evident in the excavations at the front of the cave, proximal to a number of living *Ficus* sp. plants. Post-

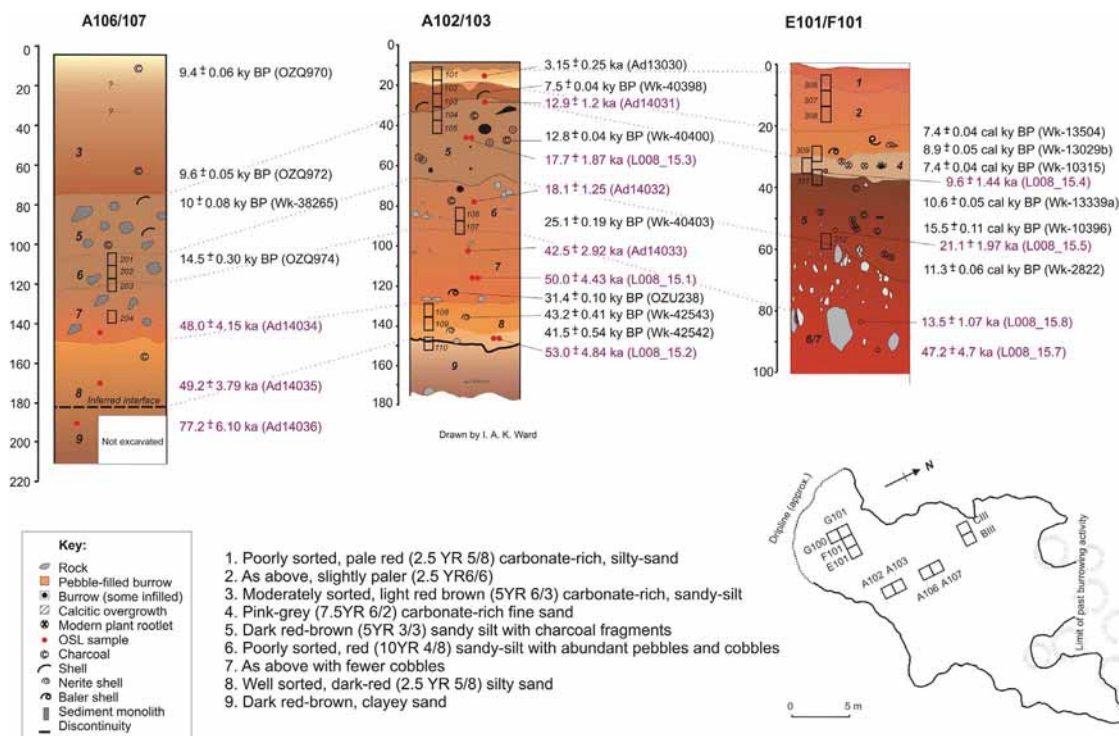


Fig. 4. Summary section profile for excavations in Boodie Cave, showing position of micromorphological samples in (A) A106/107, (B) A102/A103 and (C) E101/F101 profiles. Inset shows plan of excavations at the front of the cave.

Table 1
Chronology, palaeoenvironmental and archaeological context.
(Based on Veth et al., 2017; Ward et al., 2015, 2017.)

SU	Chronology (ka BP)	Palaeoenvironmental context	Geoarchaeological context	Archaeological context
1	1.7–2.5	Fully marine (island)	Carbonate sediments dominant — biogenic sands and limestone	Minor and small reworked cultural grains
2	2.5–6.8	Fully marine (island)	Carbonate sediments dominant — biogenic sands and limestone (moderate energy environment)	Interface between midden at entrance and largely sterile overlying sediments
3	6.8–7.2	Islandisation	Carbonate sediments dominant — biogenic sands and limestone	Dense midden unit between 6.8 and 7.2 ka
4	7.2–7.4	Islandisation	Biogenic sand dominant, little or no limestone (ephemeral event)	Mixed marine and terrestrial dietary fauna with utilitarian component
5	7.4–22.4	Transgressing shoreline	Increasing carbonate sediments; high organic content (low energy environment)	Terrestrial fauna dominant however presence of 22 Dentalium beads
6	36.6–42.6	<i>Discontinuity?</i> Regressing shoreline	Siliciclastic sediments, decreasing limestone rubble	<i>Occupational discontinuity</i> Terrestrial fauna dominant
7	42.6–46.2	Regressing shoreline	Siliciclastic sediments with coarse limestone rubble (high energy environment)	Marine pulse and dense lithics
8	46.2–51.1	Transgressing shoreline; cave open	Siliciclastic sediments dominant (low energy environment)	Hybrid and low–medium density cultural assemblages
9	~77	<i>Lithological discontinuity</i> Continental — regressing shoreline; cave closed	Siliciclastic sediments dominant (low energy environment)	<i>Occupational discontinuity</i> Sterile but with minor and small reworked cultural grains

depositional pedogenic alteration is evident in the form of rubefaction (sediment reddening) and gypsum formation, particularly along sections of SU3 in the A102/A103 excavation. In addition, evidence of decalcification is apparent from secondary carbonate around some bone fragments particularly in the lowermost units at the front of the cave.

2.2. Micromorphology sampling and impregnation methods

Blocks of sediment encased in plaster were taken from A102 (South wall) at depths of 0–34 cm and 70–94 cm (Fig. 4B), and from A106 at 100–140 cm (Fig. 4A) with the aim of obtaining representative samples from stratigraphic units 1 to 7. Sediment blocks were also taken from E101 (North wall) at 1–20 cm, 25–45 cm and 50–60 cm and F101 (East wall) at 30–50 cm (Fig. 4C), with a particular focus on sampling the unit boundaries. The sediment blocks were transported back to the UWA laboratories for processing and analysis.

Standard processes for soil thin section preparation followed Courty et al. (1989). Sediment monoliths were air dried before resin impregnation, using a mix of polyester resin diluted with styrene at a ratio of seven parts resin to three parts styrene, with methyl ethyl ketone peroxide (MEKP) was added as a catalyst at about 7 mL MEKP to 1 L resin/styrene mixture. The resin was poured on the sides of the samples and let to infiltrate slowly into the sediment, and then allowed to cure over several weeks. The hardened monoliths were sliced into chips (54 × 63 × 10 mm) using a diamond rock saw and then sent to a commercial petrographic laboratory (Spectrum Petrographics, Vancouver, Washington, USA) to be made into large (5 × 7.5 cm) thin sections, 25 to 30 microns-thick. A total of 26 thin sections were made.

2.3. Analysis methods — including petrographic, QEMSCAN®, XRD and particle size analysis

Grain size analyses were undertaken from either bulk sediment samples collected from excavation spits or from the section walls. Analyses were focused on characterising the main stratigraphic units rather than their interfaces, for which more detailed sampling would be required. Grain size analyses were also undertaken on samples of dune, beach and palaeosol sediments and from a closed cave (Ledge Cave) from north and west sides of the island. Particle size analysis (< 1 mm) included use of sieves (< 63 µm–1 mm) and also on representative samples from the A103 and E101 excavation profiles by laser particle analysis, using a Malvern Mastersizer.

Thin sections were observed at a macroscale to identify the main microfacies and/or sub-units visible in natural light. Sixteen (16) microstratigraphic units were identified within representative thin sections from the main nine stratigraphic units (see also Ward et al., 2017). These are not intended to be comprehensive of the full stratigraphic profile. All thin sections were observed using a Nikon polarizing petrographic microscope available at the Microscope laboratory in the School of Earth and Environment at UWA. Identification, description and semi-quantitative evaluation of abundance of various particles were done under plane polarized light (PPL) and crossed-polarized light (XPL) using different magnifications (2 ×, 5 ×, 10 ×, 25 ×) following terminology outlined by Stoops (2003). A summary of the micro-stratigraphy (Appendix Tables A1 and A2) and post-depositional alteration features (Appendix Tables A3 and A4) is provided in the Appendixes for inside and at the front of Boodie Cave respectively.

In addition to standard petrographic analysis, two micromorphological samples from A106 and three from F101 were selected for QEMSCAN® (Quantitative Evaluation of Minerals by Scanning Electron Microscopy) analysis. The QEMSCAN® operating system comprises a scanning electron microscope (SEM) fitted with two light-element energy dispersive X-ray spectrometers for X-ray count rate optimisation. This system provides rapid, quantitative mineralogical analyses via the automated acquisition of X-ray spectra (Butcher et al., 2000; Pirrie et al., 2004). Micron scale mineral maps are the output of the QEMSCAN® system, which provides in-situ mineralogical identification and visual representation of texture and spatial relationships of constituents otherwise only resolvable during micromorphological analyses.

Five resin impregnated sediment billets remaining from thin section production, two from A106 (samples 203 and 204) and three from F101 (samples 301, 303 and 305 from F101, which are equivalent to 309, 309 and 310 in E101) were sent to the Australian National University (ANU) for analysis. Sub-samples measuring 51 × 25 × 3 mm were extracted and analysed to correspond to each thin section. Samples were analysed using a FEI QEMSCAN 650F automated SEM-EDS system at the Centre for Advanced Microscopy (CAM) at ANU. The QEMSCAN® was run in Fieldscan mode where the surface of the sample is automatically mapped using a fixed step interval (Haberlah et al., 2011). Elemental spectra were captured using FEI iMeasure software and FEI NanoMin software was used to process raw data including refining mineral identification. A 15 µm step interval (becoming pixel spacing in the mineral map), 2000 X-ray counts per pixel and a current of 10 nA

were selected for analyses. At each pixel spacing (15 μm) an X-ray energy spectrum was rapidly acquired and compared against a database of known chemical compositions of minerals, and then its weight percent calculated. In this way, the mineral composition of each particle is systematically mapped and digital pixel maps created (Haberlah et al., 2011). Of note, porosity in the QEMSCAN[®] mineral maps may be misleading due to pore space and organic material appearing as background. Unclassified pixels can be due to non-oriented clays, the intersection of minerals within the beam width, or a mineral not present in the NanoMin mineral library. Unclassified areas can be significantly reduced during post-scan processing (Haberlah et al., 2011).

Although QEMSCAN[®] is able to clearly differentiate major minerals, it is unable to differentiate mineral species with the same chemical composition, such as calcite and aragonite. The technology is also unable to map amorphous (non-crystalline or poorly ordered) materials. Further, the identification of clay minerals can be problematic and thus major clay mineral groupings are used here to minimize potential misidentifications; namely kaolin, smectite, vermiculite, mica (illite) and chlorite. Quantified XRD was undertaken to identify the main minerals to be added to the QEMSCAN[®] mineral library in NanoMin, then other related minerals were added. Discrepancies between percentage values of minerals identified by QXRD and QEMSCAN[®] can, in part, reflect variations in the way minerals are quantified, i.e. volumetrically in QXRD (from a bulk sample) and based on two dimensional surface area in QEMSCAN[®]. Given sample heterogeneity — some discrepancies between the two methods for assessing mineral composition would be anticipated (see also Edwards et al., 2017).

For the XRD analysis, two disaggregated sub-samples (5 g) were taken from monoliths (106B and 303). These samples were further divided and prepared for XRD analyses of both bulk sample and clay fraction following methods described in Moore and Reynolds (1997). For identification of clays sub-samples were sieved through a double nest (500 μm then 100 μm mesh) before settling overnight. This additional step was required due to the coarse nature of the sediments. After settling, the Ostrom method (1961) removed carbonates from clay samples to achieve clean and sharp peaks in the XRD spectra. Samples were then rinsed and centrifuged twice (Spintron GT-50F) with 291 g of

deionised water for intervals of 10 min before using the Millipore Filter Transfer Method (Moore and Reynolds, 1997). A SIEMENS D5005 Bragg-Brentano diffractometer (reflection geometry) equipped with a graphite monochromator and scintillation detector was used, with *CoK α* radiation, a scan range of 4–84° 2 θ for bulk and 4–32° for clay samples, at a step width of 0.02° and a scan speed of 2 s per step. Results were interpreted using the Bruker AXS software package Diffracplus Eva 10 (2003) for identification, and Siroquant V3 for quantification (using the bulk scan).

3. Results

3.1. Grain size analyses

In order to help understand the depositional context for the archaeology, the sieve data for the > 4 mm and 4–2 mm sediment fractions collected in the field was collated and normalised in terms of density (Fig. 5). The density of coarse (> 2 and > 4 mm) sediments was generally higher in the more exposed E101/F101 profiles and lower in the more sheltered A106/107 profiles (Fig. 5). In the A106/107 profile, the sediments are increasingly coarse from SU6/5 upward, which alongside the decreased stratigraphic differentiation and a similar chronology (Fig. 4) suggests these units have experienced some degree of mixing (see also Veth et al., 2014). There is a very strong positive correlation, particularly in the density of the > 4 mm fraction with total sediment density.

Grain size trends in the A102/103 profiles are more consistent. In the base of the Boodie Cave profile, in SU9/8 of the A103 profile, the sediments are finer-grained, reflecting a more closed system dominated by in situ weathering of the cave; dated at SU9 to 77 ka (Veth et al., 2017; see Fig. 6). The coarse rubble (> 4 mm) component of the cave sediments increases significantly in SU7 both inside the cave and at the front in E101/F101 (Fig. 5) indicating probable roof-fall event(s). This event(s) likely opened up the cave and allowed a greater input of exogenous (reworked dune) sediments. Between SU6–SU3, a lower but relatively constant density of around 0.1–0.2 g/cm³ in the > 2 mm component of the sediments indicates sedimentation is of lower energy

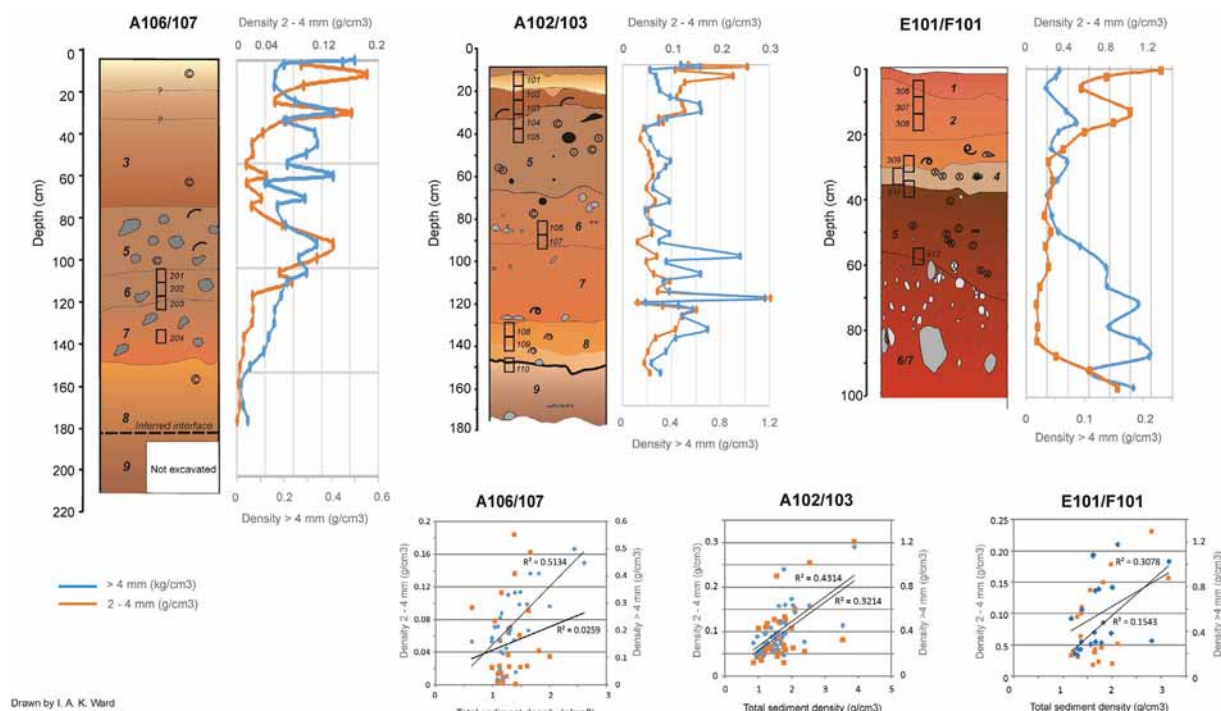


Fig. 5. Depth profiles and density correlations for > 4 mm and 2–4 mm sediment fractions inside the cave in A106/107, A102/A103 and at front of cave in E101/F101. Results show overall positive correlation of coarse sediment fraction with total sediment density.

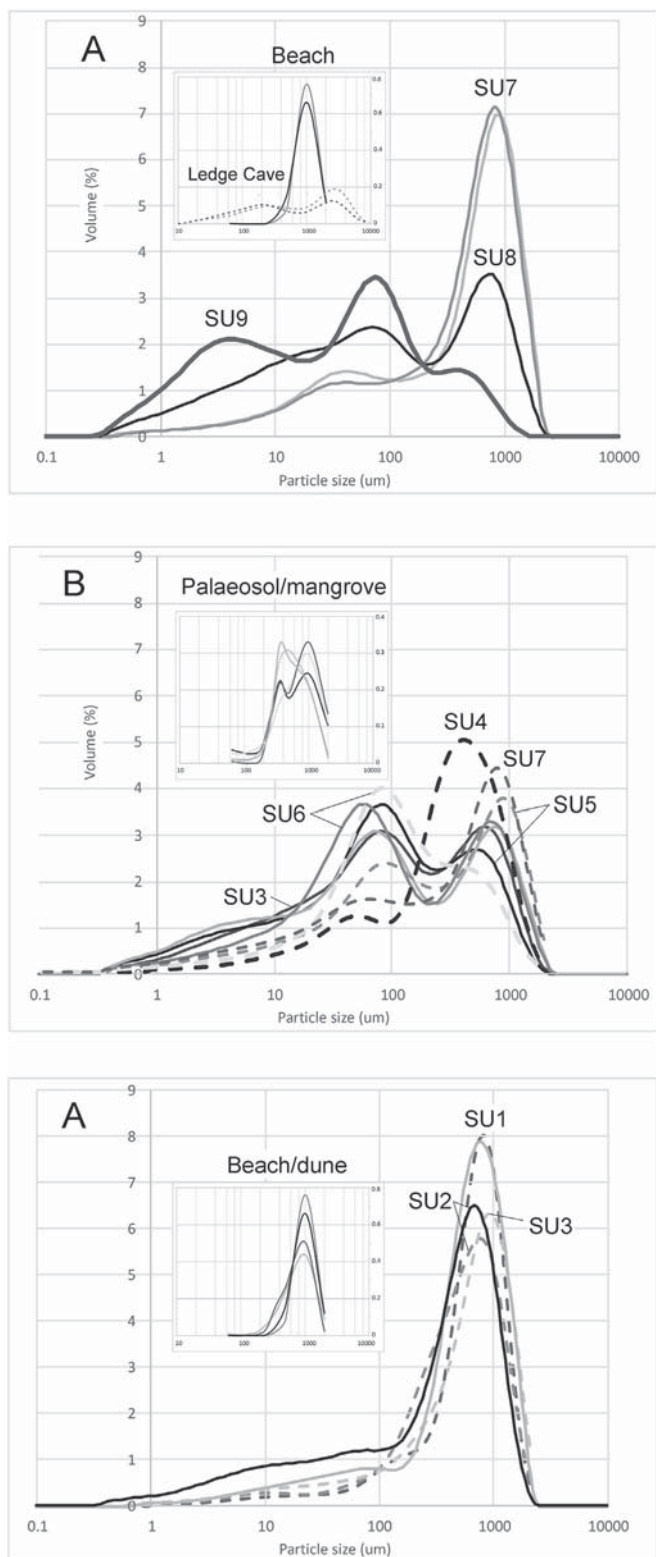


Fig. 6. Overview of grain size for each of the stratigraphic units inside the cave (unbroken lines) and at the front of cave (dashed lines) (as determined from laser particle size analysis), with inset figures showing grain size analyses (as determined from sieve analysis) of sediments from local environmental contexts on Barrow Island, including a closed cave (Ledge Cave), beach, dune, mangrove and palaeosol sediments.

and less erratic. In both the front and inside the cave, the > 4 mm and more especially the 2–4 mm components increase from SU3 to 1 indicating higher energy depositional processes. As noted for the A106 profile, there is a strong positive correlation in the density of both the

2–4 mm and > 4 mm fractions with total sediment density, which may be an important consideration for profiling depth trends in artefact density.

The < 2 mm sediment fraction generally comprises coarse (0.5–1 mm) and medium (250–500 μm) sands, with varying proportions of carbonate and silicate fractions down through the profile. Beginning inside the cave with the basal unit, SU9, this shows a trimodal distribution with peaks at 4 μm , 70 μm and 370 μm . This is inferred to represent in situ degraded clay material from the cave itself, at a time when the cave was largely closed to the external environment. Above this, units SU8 and SU7 show a coarse (760–820 μm) unimodal distribution that is more typical of dune sands (Fig. 6A), implying a different sediment source at this time.

Inside the cave, the intermediate units generally contain less pebble-sized material (Fig. 6B). In the < 2 mm fraction, units SU6, SU5 and SU3 are strongly bimodally skewed towards the finer grain sizes, with a distinct silt-sized modal peak around 75 μm and a coarse peak (predominantly limestone and some bone) between 570 and 850 μm (Fig. 6B). This reflects a greater relative percentage of wind-blown material in these sediments. Comparison with palaeosol samples and sediments typical of mangrove swamps around Barrow Island shows a similar bimodal distribution, indicating these sediments are likely reworked from one or more sources that may include mangrove environments. For SU4, which is present only at the front of the cave, the peak modal grain size at 390 μm largely reflects biogenic carbonate rather than degraded limestone.

The pebble component, particularly in the 2–4 mm fraction, increases in the uppermost sediments. In the upper two units (SU1 and SU2) and also in SU3 in the front of the cave, the < 2 mm sediment fraction comprises unimodal coarse (720 μm) carbonate-rich sands, with a minor siliciclastic fraction (Fig. 6C). The particle size is similar to that of modern beach and dune sands, which are also predominantly unimodal and coarse grained (500 μm –1 mm) (Fig. 6C inset). The contrasting bimodal grain size distribution for SU3 inside the cave possibly reflects greater relative bioturbation, a greater contribution of sand at the front of the cave, and/or some other process. Whatever the cause, the relative difference in source and/or process inside and outside the cave is absent in the upper two units.

3.2. Contacts and interfaces

Microstratigraphy provides the minimum archaeological stratigraphic unit that can be used in the analysis and interpretation of a palaeolandscape at the local or regional scale. Key to defining these units/sub-units are the boundaries, some of which are sharp at both the macro- and micro-scale, whilst others are more gradational. The deposit is generally horizontally oriented. The following describes the macro-scale and micro-scale contacts between the main stratigraphic units, beginning from the oldest part of the sequence. It should be noted that these contacts are not necessarily present across every square — indeed A106 shows little or no stratigraphic variation except from SU6, hence the following is a synthesis of unit boundaries across all five excavations.

Inside the cave, the transition from SU9 to SU8 is quite subtle, marked at the macroscale by finer, red (2.5YR 4/6), moderate to well-compacted sediments (Fig. 7A). At the meso- (Fig. 7B) and micro-scale (Fig. 7C(b)), the unit interface is quite even and sharp, marked by a sedimentary seal or crust of iron-oxide rich sediments against which the less compact sediments of SU8 have accumulated. This may be indicative of an erosive surface or disconformity. Within SU8, a subtle colour change from 2.5YR 5/8 to 2.5YR 4/6 (i.e. slightly lighter) *within* parts of the unit (labelled as SU8B and A respectively), indicates possible localised leaching of sediments. In contrast the transition from SU8 to SU7 is a gradual conformable contact (Fig. 7A), though again marked by slightly darker, moderately compacted sediments (2.5YR 4/8) and an increase in cobble-sized material (probably roof-fall). At the

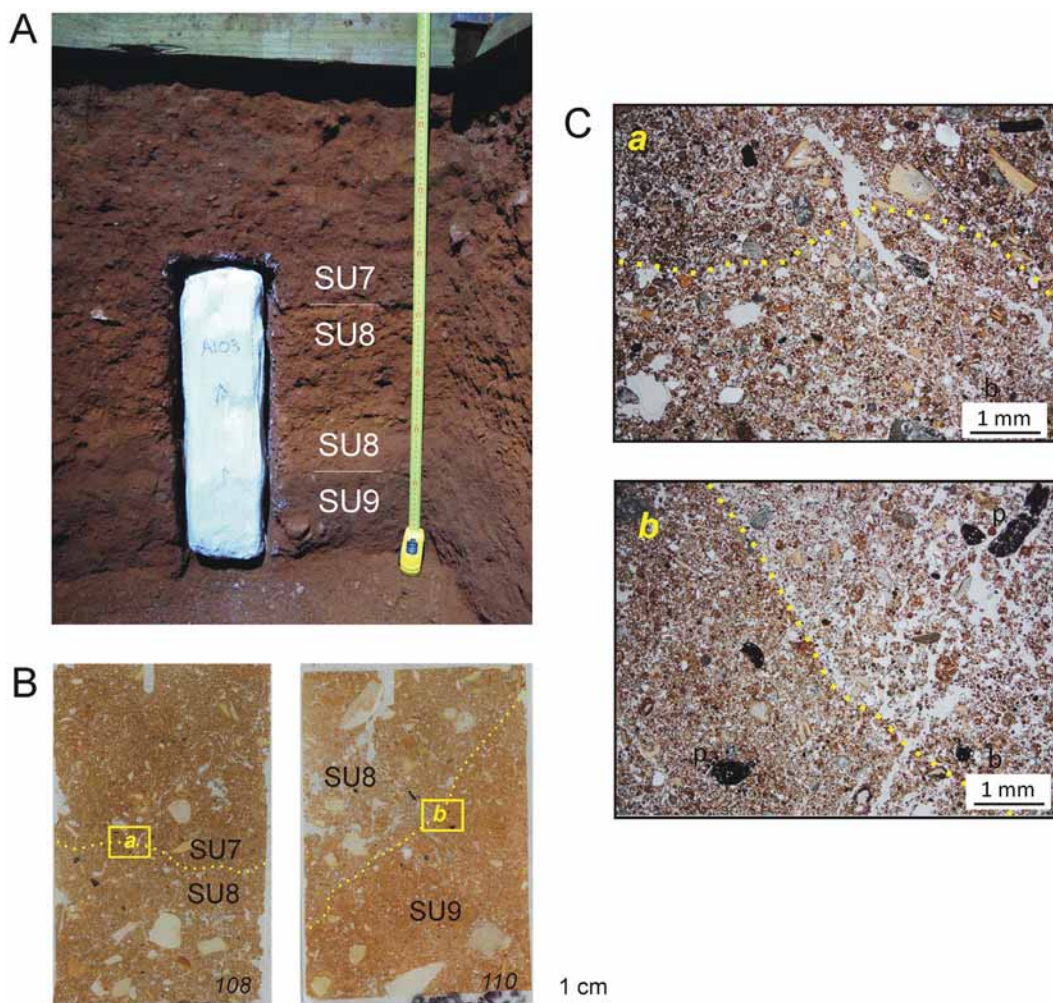


Fig. 7. Profile of A103 excavation (South wall) showing position of stratigraphic boundaries for SU9/SU8 and SU8/SU7 at the (A) macro-, (B) meso- and (C) microscale. The interface between SU8 and SU7 is clearer at macro-scale, whilst the interface between SU9 and SU8 is sharper at the meso- and microscale, where there is a textural difference in the more compacted sediments of SU9. (For interpretation of the references to colour in this figure, the reader is referred to the web version of this article.)

microscale, the uneven interface is evident from a much higher iron-oxide content and the presence of larger bone fragments in the SU7 sediments compared to SU8.

Still inside the cave, in both A102 (Fig. 8A, B) and A106 (Fig. 9A, B), there is a gradual conformable contact between SU7 and SU6. The gradual and uneven contact between SU7 to SU6 inside the cave is marked at the macroscale by slightly duller sediments (from 2.5YR 4/8 to 2.5YR 4/6) and patches of cobbles (Fig. 8B, cf. Fig. 4B), and at the microscale by the contrasting high iron-oxide content of SU7 (Fig. 8C and 9C). In contrast, at the front of the cave the abrupt conformable contact between SU7/6 and SU5 is evident both at the macro- (Fig. 10A), meso- (Fig. 9B) and micro-scale by a marked decrease in cobble and pebble-sized fragments, and by the darker but less intensely red sediments (from 10YR 4/8 to 5YR 3/3). The latter reflects a higher organic content, as evident from the presence of randomly distributed fragments of charcoal (2 mm–1.5 cm), largely explaining the difference in colour with the same unit inside the cave.

From the base of SU5 (i.e. 5C) through to the top of the unit (i.e. Fig. 5B and A) there is a significant decrease in quartz and feldspar, an increase in biogenic carbonate in the sediments and a slight but notable increase in number of burnt bone fragments (Table A3 and A4). Inside the cave, in A102, gypsum is also present in the thin section from the top of the unit. Here the transition from SU5 to SU3 is largely obscured by gypsum overgrowth along the East, South and West walls, except on the North Wall where the interface is visible from a subtle colour

change (from 2.5YR 4/6 to 5YR 4/6, i.e. slightly more red).

Another abrupt conformable contact occurs between SU5 and SU4 at the front of the cave, marked by a colour change to light pink-grey (7.5YR 6/2), well-sorted sandy sediments with abundant marine fauna, including a distinct lens (~2 cm thick) of echinoderm ossicles and a near-absence of microbone fragments (Fig. 10A, B). At the microscale (Fig. 10C(c)), the interface is uneven with some reworking of biogenic fragments across the SU5/SU4 interface. Although comparatively thinner than most other units (< 10 cm), micromorphology shows at least three microfacies – or midden-building events – within SU4, with the lower sub-unit (4C) defined by a high concentration of echinoderm ossicles and iron-oxides and the middle sub-unit (4B) defined by almost pure biogenic sand with no limestone fragments.

Above this is another abrupt conformable contact between SU4 and SU3 (Fig. 10A, B and C(b)) with a relatively sharp and even interface, displaying a compositional change from the predominantly biogenic sands to looser, ferruginous, mixed limestone and biogenic carbonate sediments. In contrast, the contact between SU3 and SU2 is more of a gradual conformable contact, visible mainly from the subtle change to more dry, loose, light red sediments both inside (5YR 6/6) and at the front (2.5YR 6/6) of the cave. At the microscale, only a slightly higher concentration of ferruginous quartz carbonate sand is evident at the SU3/SU2 interface, otherwise there is only minor textural and compositional difference within and between these units.

The final transition from SU2 and SU1 appears relatively

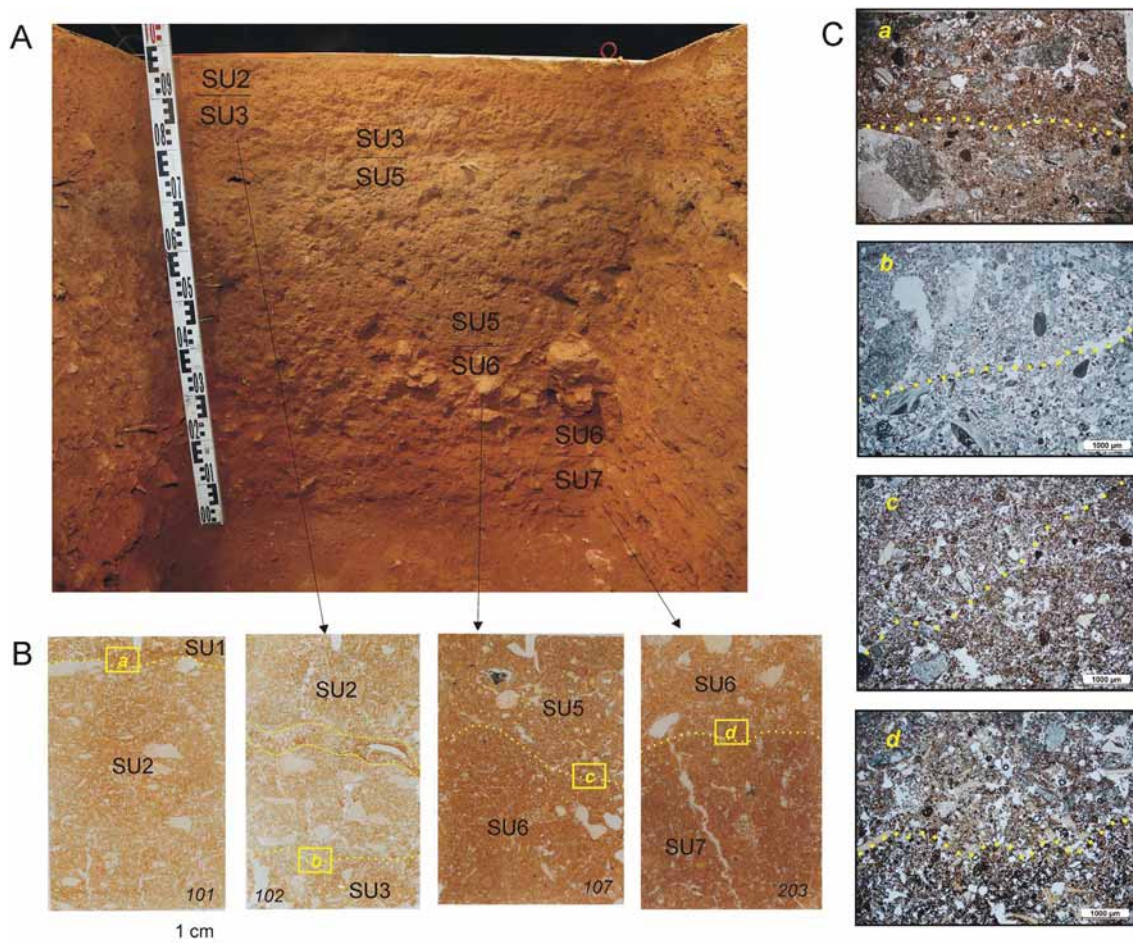


Fig. 8. Profile of A102 excavation (North wall) showing position of stratigraphic interfaces for SU6/SU5, SU5/SU3 and SU3/SU2 at the (A) macro-, (B) meso- and (C) microscale. In most cases unit interfaces are better defined at the microscale where there are visible compositional and textural differences between units. (For interpretation of the references to colour in this figure, the reader is referred to the web version of this article.)

gradational at the macroscale (Fig. 8A and 10A), once again marked by increasingly dry, unconsolidated sediments and a subtle increase in intensity of colour to 5YR 5/8 and 2.5YR 5/8 inside and at the front of the cave respectively. However, at the meso- (Fig. 8B and 10B) and microscale (Fig. 8C(a) and 10C(a)) the interface is more abrupt. Inside the cave especially, in A102 (Fig. 10C(a)), a microlayer (~500 µm thick) of fine ferruginous sands – SU 1B – occurs below the more poorly-sorted coarse limestone-rich sediments of SU1. This microlayer may represent a sedimentary seal or crust, indicative of a former surface.

3.3. QEMSCAN® and XRD analyses

QEMSCAN® analyses provide a visual representation at the meso-scale of unit composition, texture and interfaces. Two stratigraphic sequences were sub-sampled for QEMSCAN® analysis: SU3 to SU5 at the front of the cave (samples 301, 303 and 305 from F101) and SU6 and SU7 within the cave (samples 203 and 204 in A106). The results are presented from oldest to youngest. SU7 is represented in sample 204 (A106-4) and the base of sample 203 (A106-3) from within the cave (Fig. 11a, b). The unit is primarily well-sorted and comprised of sub-rounded, very coarse to fine, quartz sand (~60%), with some grains of feldspar (~14%). A thin (< 1 cm) lens of quartz was observed in thin section (Fig. 9C), and probably represents a brief in-wash event; unfortunately this was not present on the other half of the billet sampled for QEMSCAN® analysis. The density of bone increases dramatically in the upper few centimetres of this unit, from ~4% in sample 204 to ~20% in the base of sample 203. Similar trends were observed from

petrographic analyses, with the addition of plant fragments (Table A1). The predominant clay mineral, like other units, is mica (illite), accounting for ~15% of identified minerals. Although identified in petrographic analyses (Table A1), QEMSCAN® indicates SU7 is devoid of calcite, except in the upper few centimetres of the unit. The quartz-dominated sand is likely aeolian.

The transition between SU7 and SU6 is present in sample 203 (A106-3). The sediment matrix between the two units is similar, except for the presence of sub-angular calcite fragments of various size categories that comprise approximately 40% of SU6. Estimates for calcite were lower (20%) from petrographic analyses (Table A1). Otherwise similar trends are observed in thin section, with lower percentages of quartz and feldspar and higher densities of bone in the upper portion of SU7 also present in the base of SU6. Effectively, there are continuities in the deposition of finer material (including mica) from SU7 to SU6; however, there is a marked shift from the absence of calcite in SU7 to the abundance of locally-derived limestone in SU6.

SU5 is represented in sample 305 (Fig. 12A) and the base of sample 303 (Fig. 12B). The unit is a poorly sorted admixture of local and extra-local materials. The sub-rounded calcite fragments are presumably of local derivation, although the sub-rounding is suggestive of transportation. The fine fraction is dominated by ~40% quartz sand (varying from very coarse to very fine) and ~20% bone (apatite), with an admixture of minor primary and secondary minerals including feldspars, amphiboles and pyroxenes. The upper few centimetres of SU5, at the boundary with SU4 in the base of sample 303, are characterised by an upper zone of denser fine matrix directly above a zone with an

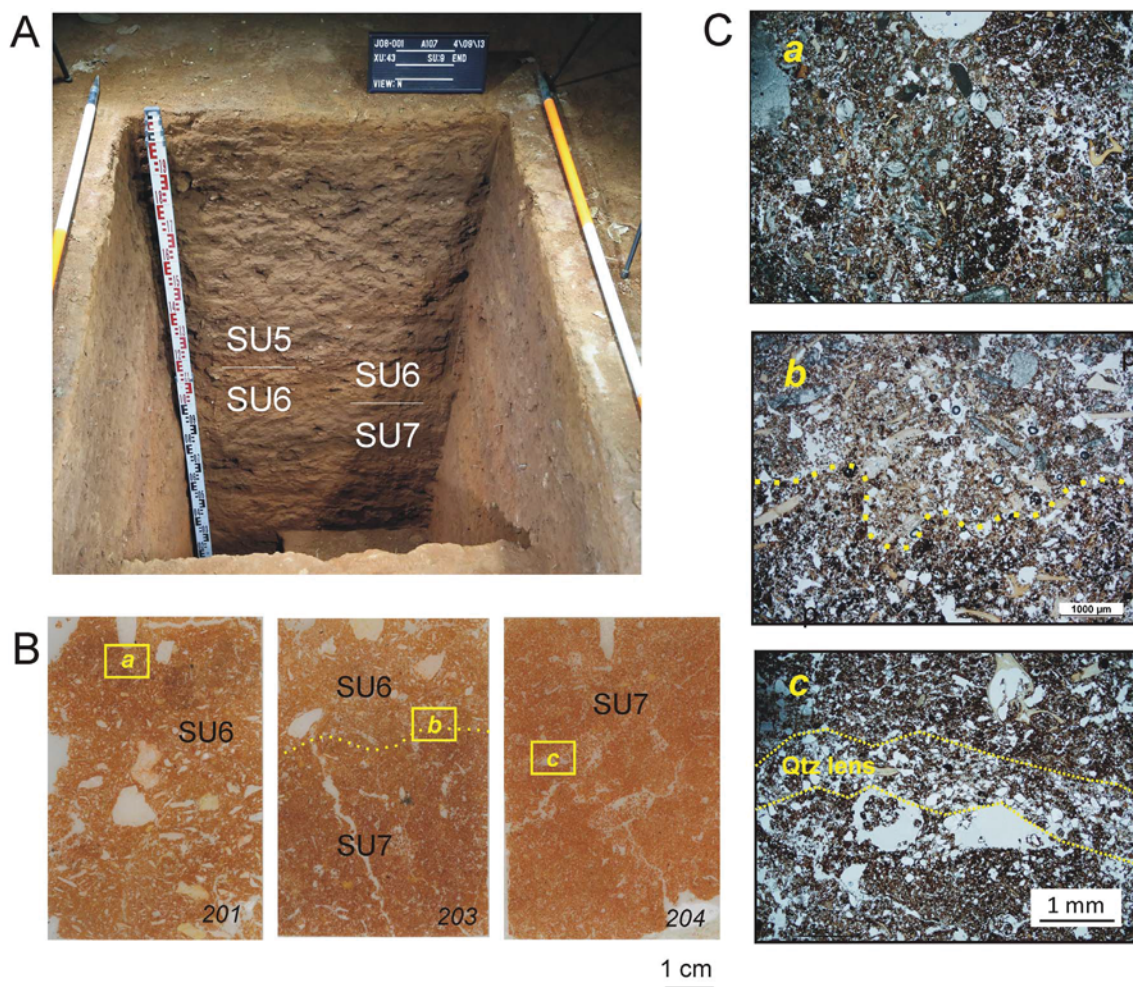


Fig. 9. Profile of A106 excavation (South wall) showing stratigraphic interfaces for SU7/SU6 and SU6/SU5 at (A) macro-, (B) meso- and (C) microscale. Microscale images show (a) excrement fabric in SU5, (b) interface between SU7 and SU6, (c) quartz lens within SU7. (For interpretation of the references to colour in this figure, the reader is referred to the web version of this article.)

increased number of horizontally oriented clasts (calcite and bone fragments) (Fig. 12B). A similar zone between SU5 and SU4 was also observed in the equivalent 311 thin section from E101 (Fig. 10B). Although each zone is only 1–2 cm thick, taken together they may be suggestive of a former ground surface, with comminution of material and possibly trampling. The transition from SU5 to SU4 is marked by a switch from quartz-dominated to calcareous-dominated sand fraction (Fig. 12B).

SU4 is present in the upper half of sample 303 and the base of sample 301 (Fig. 12C). The majority of the unit is comprised of moderately-to-well sorted sand, with rounded grains of calcareous sand dominant (>60%) and sub-rounded grains of quartz sand minor (<10%). The majority of the unit is homogenous; there does not appear to be any internal stratification. This contrasts with petrographic analyses which show a concentration of echinoderm ossicles at the base of Unit 4 (Table A1; see also Ward et al., 2017). An exception in the QEMSCAN® analyses is approximately 1–2 cm below the boundary with SU3 where there is a zone of aligned and gently inclined calcite and bone fragments (Fig. 12C). These oriented clasts plausibly suggest a former ground surface and may plausibly be indicative of trampling. Trampling in the upper part of SU4 is also implied from broken bone fragments (Fig. 13G; Table A1).

SU3 is present in the upper two-thirds of sample 301 (Fig. 12b). The unit is poorly sorted and dominated by angular calcite fragments of varying size and orientation. The fine matrix between clasts comprises admixed calcite and quartz sand with bone and shell fragments, as well

as very minor clay (<2%). The large, angular clasts of calcite are presumably locally derived limestone. These QEMSCAN® results complement a similar automated mineral analysis using Tescan Integrated Mineral Analyser (TIMA®), which revealed a gradual change from a polyminerologic quartz-rich assemblage spanning ~50–12 ka to a more simple carbonate-dominated assemblage from the terminal Pleistocene <12 ka (Ward et al., 2017).

3.4. Biogenic and anthropogenic features

3.4.1. Bone

Fig. 13 shows different bone fragments observed in thin section, with the majority from SU5 where abundance of bone fragments – both burnt and unburnt – is highest (15–40%). This contrasts with the macroscale record where SU3 has the highest abundance and diversity of zooarchaeological remains, including mammals, reptiles and fish, all of which are extremely well preserved (Manne et al., 2017). The microscale record shows that the main alteration of bone is impregnation of Fe- and Mn-oxides (e.g. Fig. 17G, J, M) and carbonate encrustation (Fig. 13C, D). Encrustation is fairly uniform around bone fragments, implying it is related more to general soil moisture conditions rather than preferential movement of water down the profile (as might be indicated from cappings or pendants). This mineralisation was also observed at the macro-scale and was more prevalent at the front of the cave.

In the uppermost sediments, fragments of chitin are also observed



Fig. 10. Profile of E101 excavation (East wall) showing position of stratigraphic interfaces between SU7/SU5, SU5/SU4, SU4/SU3, SU3/SU2 and SU2/SU1 at (A) macro-, (B) meso- and (C) microscale. Unit interfaces are evident at all scales but are sharpest for the lower units where there is both textural, compositional and colour difference between units. (For interpretation of the references to colour in this figure legend, the reader is referred to the web version of this article.)

(Fig. 13A, B) and most likely derive as excrement-products from microbats (*Vespadelus finlaysoni*) that live on the cave ceiling. Chitin is not observed deeper in the sequence, more likely reflecting lack of preservation than absence of microbats. Fig. 13E and F show lightly burnt bone fragments, which in PPL are orange in colour and which in SU5 sometimes occur alongside fragments of carbonised plant material. The abundance of burnt bone material in thin section is not high (< 5%, Table A3 and A4) and there is very little ash associated with it, indicating low-temperature burning. In addition to bone, there are also teeth in SU5 (Fig. 13I), some of which are also burnt (Fig. 13J). In the macro records, the majority (95%) of burnt material was carbonised (black) rather than fully burned, again indicating low levels of burning (Manne pers. comm.).

Fracturing was observed in some long microbone fragments, such as shown in Fig. 13G and H from SU5, which is seen to be indicative of trampling. Increased fragmentation of macrobone fragments, albeit still with good preservation, was observed in the middle squares at the front of the cave and is similarly interpreted as a result of increased trampling by human traffic (Dooley pers. comm.). Otherwise most bone fragments show relatively angular edges (i.e. little rounding), suggesting weathering and transport is minimal.

3.4.2. Charcoal and plant material

Like bone, the majority of wood charcoal fragments – both macro and microscale – occur in SU5. These generally range from class one fragments, exhibiting preserved cellular structure (e.g. Fig. 14A, B, C), to class two or three fragments, where there is little or no cellular structure (Fig. 14D–G). Despite the preservation of structure, identification of plant species is limited by only having a single cross-section and the generally high levels of decomposition of the plant fragment. Anthracological analyses indicate hearth charcoal from *Acacia*,

Eucalyptus, *Ficus* and *Brachychiton* genera. Their presence within the macroscopic charcoal remains indicates their use was anthropogenic, brought into the cave by past occupants for fire fuel. Most of the wood charcoal recovered showed evidence for mineralisation (Fig. 14H, I), as also evidenced from field and laboratory observations that most charcoal fragments sank during flotation due to mineralisation.

Despite the abundance of charcoal in SU5, there appears to be little ash in this or any other unit. Under low-temperature conditions, production of charcoal is favoured over ash, especially when combustion is halted by smothering with sediment or dousing with water (Mentzer, 2014). At the same time, decalcification and fine-scale reworking (e.g. by insects) could have undermined preservation of ash (which is mostly calcite) in these sandy sediments. Decalcification and dissolution features are evident as mammillate edges on some limestone fragments in SU5 (Fig. 17K) and also in the units below this (Fig. 17S). Both low-temperature burning and post-depositional alteration of combustion features are likely.

The only other forms of plant material observed were a few disaggregated herbivorous dung fragments in the uppermost sediments (SU1 and SU2). This is predictable given the contemporary presence of omnivorous burrowing bettong (*Bettongia lesueur*) and likely use of the cave by other marsupials. However, such organic matter does not exist or has not been preserved in the underlying units.

3.4.3. Shell and microfossils

Marine shell and microfossils occur in most units, the majority of which are fragmented but with some whole microfossil samples. This matches the macro-malacological record, which shows fragmented shell including water worn shell fragments (mainly in SU4). A difficulty is sometimes distinguishing transported contemporary material (e.g. Fig. 15A) from fossil material that may have degraded out of host rock

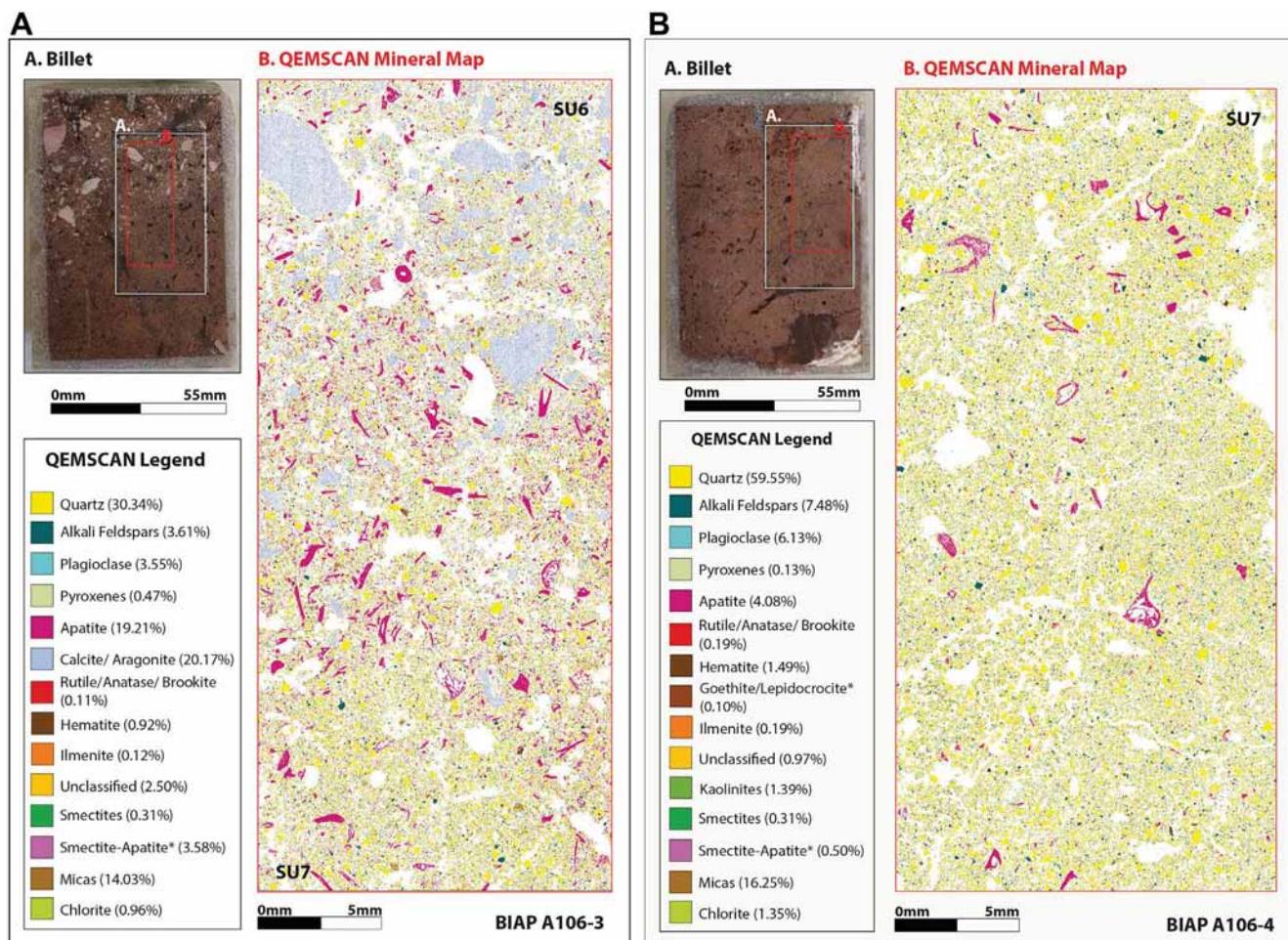


Fig. 11. QEMSCAN mineral maps for sub-samples within A106 billet, equivalent to the micromorphological thin sections of (A) 203 (left) showing the transition from SU7 to SU6, and (B) 204 (right) representative of SU7.

(e.g. Fig. 15H). In general fossil material tends to be solid rather than porous, with fewer diagnostic species, although occasional examples of *Nummulite* sp., *Rotalid* sp., *Marginopora* sp. and coral can be observed within some large fragments of limestone. No economic species (e.g. *Melo* sp., *Terebralia* sp., *Nerita* sp., etc.) are observed in the fossil shell material.

There is also the potential division between cultural shell material – both economic (Fig. 15B) and utilitarian (Fig. 15E) – and purely biogenic carbonate material (Fig. 15G). As may be expected, the highest concentration of marine shell and microfossil material occurs in the densest midden units (SU3 and 4). Here the biogenic carbonate fraction includes coral, echinoderm, foraminifera, pelloids and some molluscan and bivalve shell fragments. Cultural shell material includes echinoderm, gastropods (possibly *Terebralia* sp.) and baler (*Melo* sp.), the former as a food resource and the latter utilitarian. Archaeomalacological analyses show a dominance of *Terebralia* sp. in this midden layer, and clear evidence of baler shell implement manufacture alongside other utilitarian species including *Tridachna* sp. (giant clam) and *Dentalium* sp. (tusk shell). Cross-sections of echinoderm ossicles are observed cut horizontally or obliquely, the latter showing intricate patterning (Fig. 15I). The dark colour of some of these ossicles (e.g. Fig. 15I) is not a result of burning but rather a result of being in the intertidal zone for a period of time before being transported into the cave (Powell et al., 2011). The highly-fragmented shell generally is also indicative of reworking prior to deposition, with biogenic sands showing open rather than close packing (with no particular orientation) and no obvious evidence of trampling.

Eggshell, either avian or reptilian, also occurs in most units (Fig. 15F), albeit at low abundance (< 5%), hence may be of cultural or non-cultural origin. Similarly land snails (probably *Rhagada* sp.) occur throughout all profiles but are not considered economic. Shell tends to show little or no post-depositional alteration beyond fragmentation and micritisation, both of which may have occurred prior to deposition (i.e. occurred through impact and abrasion within the nearshore environment prior to deposition within the cave). There are some exceptions, such as in Fig. 15A, where iron-oxide hypocoatings have developed on the surface of a coral fragment but these tend to be discrete rather than ubiquitous in any sedimentary unit. Baler, larger bivalve and gastropod fragments and echinoderm can be seen clearly in the sections as included cultural grains.

3.4.4. Stone artefacts

The Boodie Cave stone artefact assemblage is largely manufactured from locally sourced silicified limestone and calcrete (Veth et al., 2017). Some non-local materials (e.g. quartz, silicified sandstones and mudstones) are also present but these lithologies only occur in small proportions. Stone artefacts are present in all units with dietary assemblages (SU3–SU8, but are most abundant in SU5) and occur in all size fractions (i.e. < 1 mm to > 4 mm). The stone artefact assemblage in Boodie Cave is large, with over 6000 artefacts in A102 and A103 alone (Veth et al., 2017). Despite this abundance, stone artefacts are difficult to distinguish in micromorphological cross-sections, mainly because Boodie Cave is composed of the same Trealla Limestone – albeit a finer-grained version (available in nearby creeks) – from which many of the

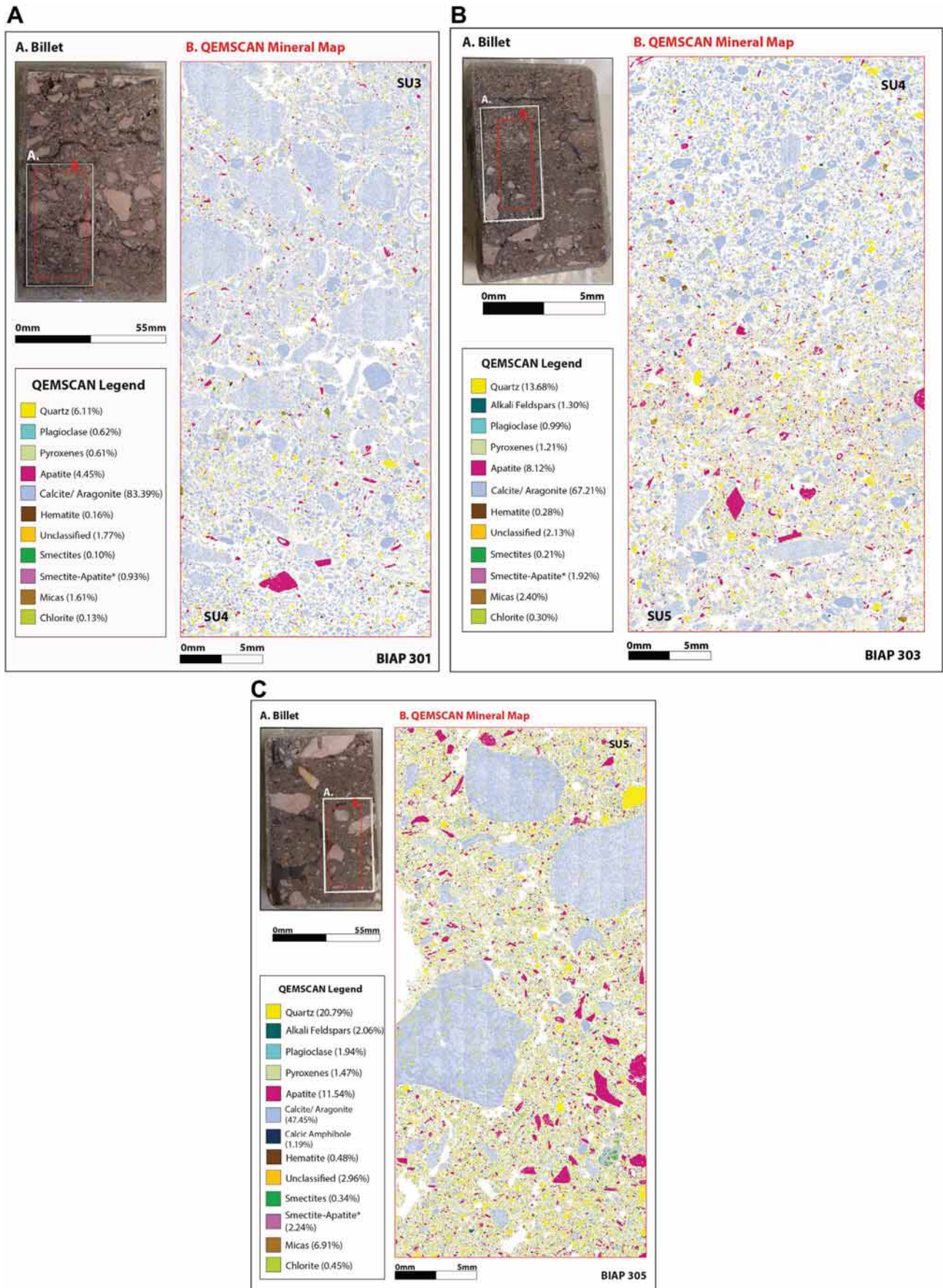


Fig. 12. QEMSCAN mineral maps for sub-samples within F101 billet, equivalent to the micromorphological thin sections of (A) 301 (upper left) showing the transition from SU4 to SU3, (B) 303 (upper right) showing the transition from SU5 to SU4, and (C) 305 (bottom) showing SU5.

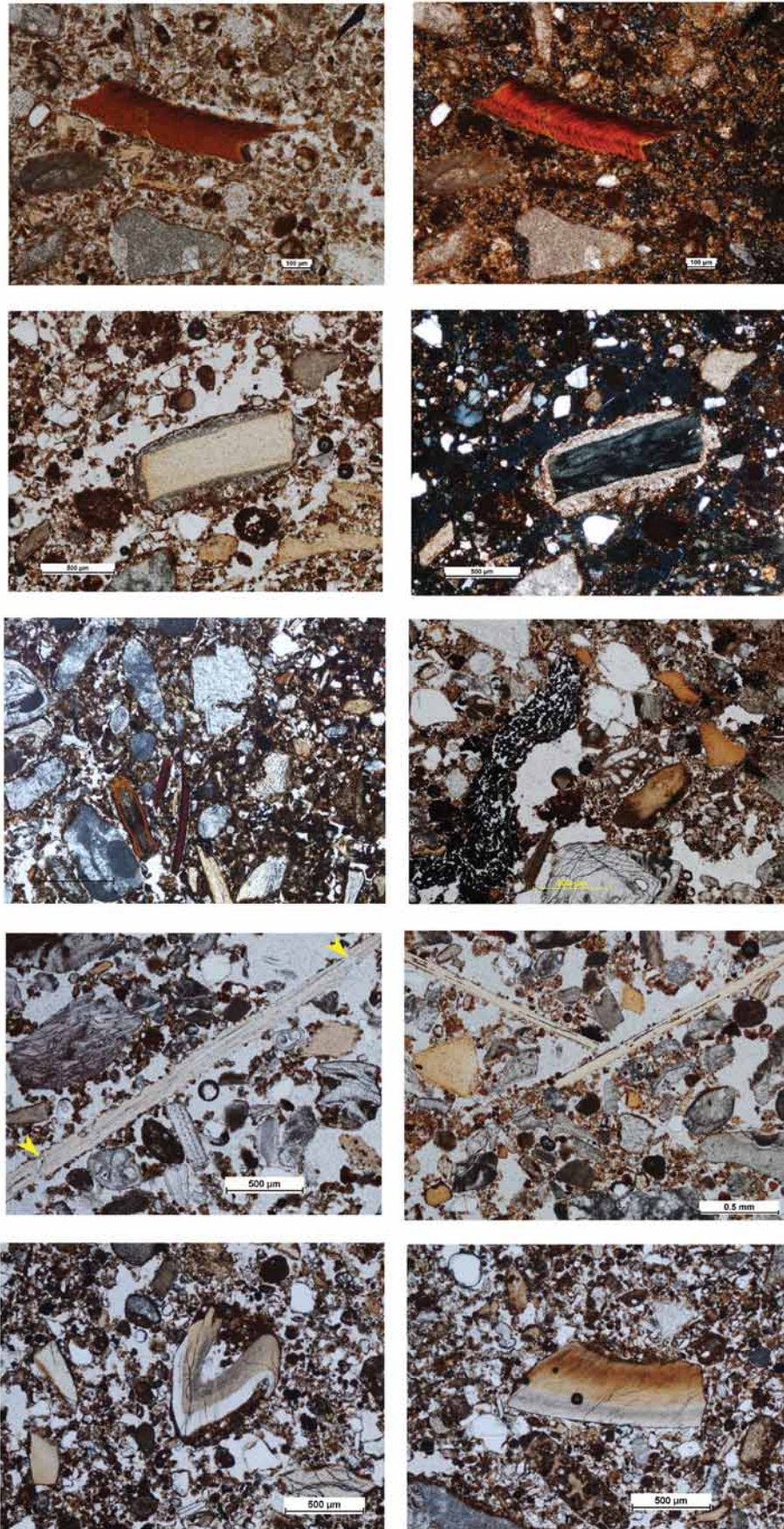


Fig. 13. Examples of bone and teeth in the Boodie Cave sediments, including (A) chiton (PPL) in SU1 and 2, (B) as for A under XPL, (C) bone fragment with secondary carbonate precipitation from SU5 (PPL), (D) as for C under XPL, (E) burnt bone fragments from SU6, (F) burnt bone fragments (and plant pseudomorph) from SU5, (G) trampled burnt fragment from SU4, (H) trampled bone fragment from SU3, (I) tooth fragment (possibly marsupial) from SU6, and (J) burnt tooth fragment from SU5. (For interpretation of the references to colour in this figure legend, the reader is referred to the web version of this article.)

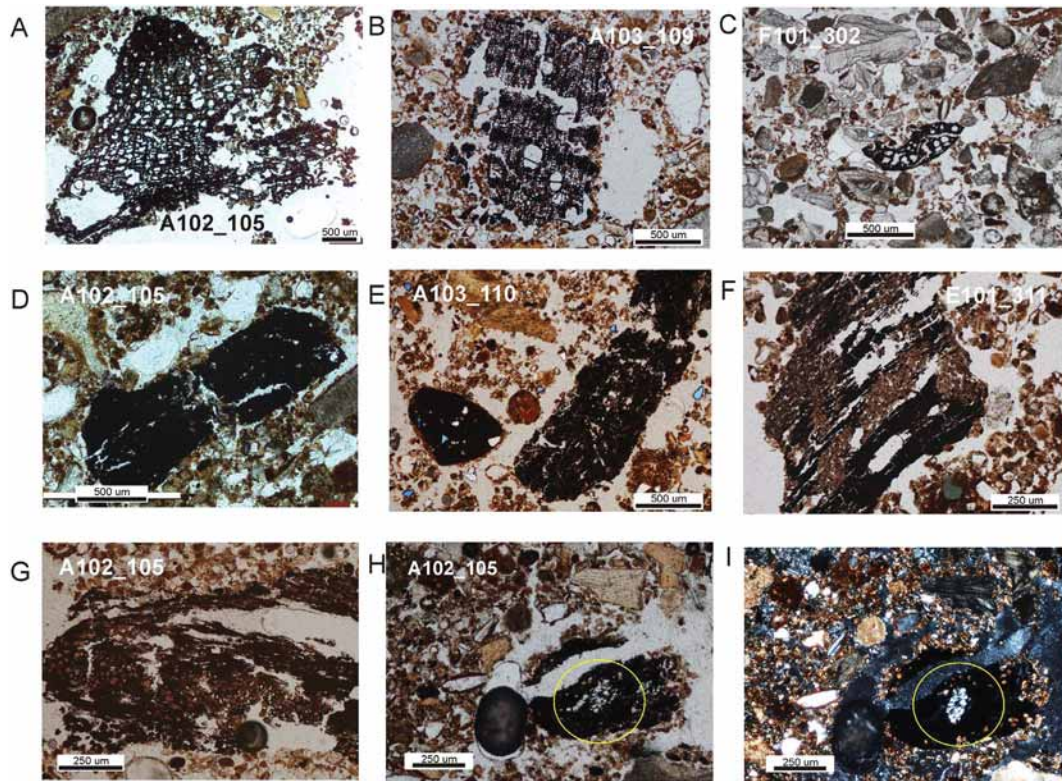


Fig. 14. Examples of plants fragments and plant pseudomorphs from Boodie Cave. The majority of these do not show identifiable features to be able to classify them by family or species but independent anthracological analyses indicate these are likely to be *Acacia*, *Ficus* and *Brachychiton* species. Class 1 plant fragments from (A) SU5, (B) SU8, (C) SU4; Class 2/3 fragments from (D) SU5, (E) SU8, (F) SU5, (G) SU5; and recrystallisation in plant fragment, within a micritic groundmass, from (H) SU5 (PPL) and (I) SU5 (XPL).

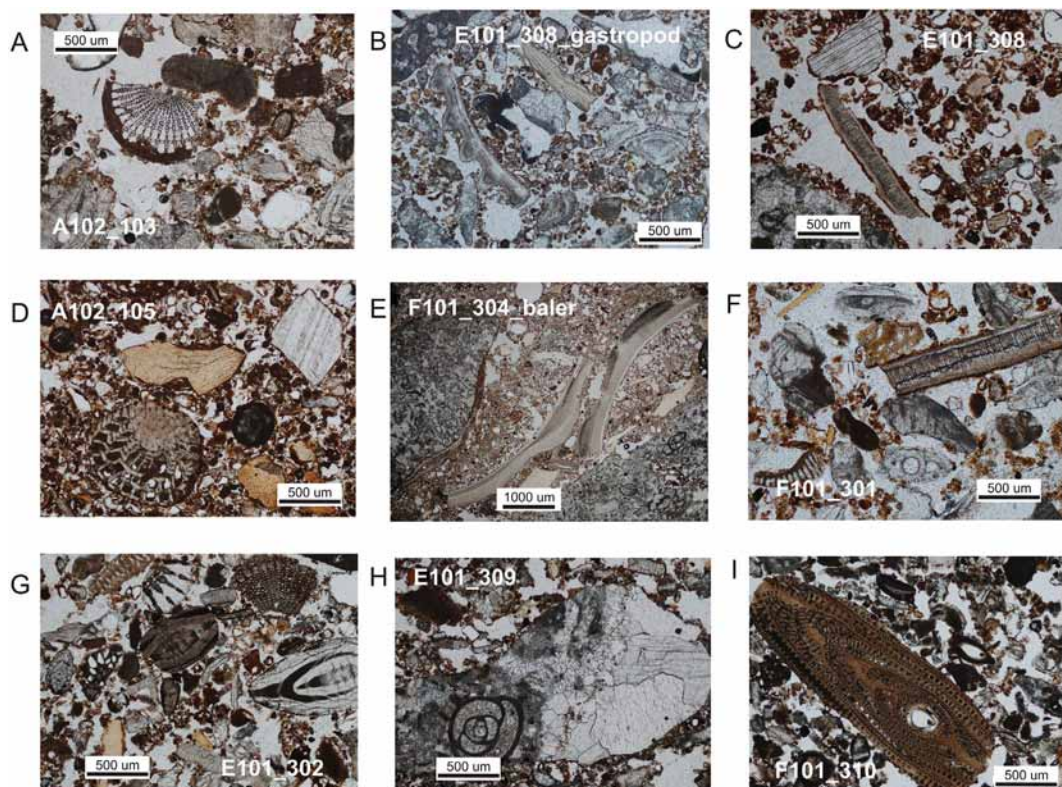


Fig. 15. Examples of shell fragments from Boodie Cave, including (A) coral fragment from SU5, (B) gastropod from SU2, (C) eggshell from SU2, (D) shell (?) from SU5, (E) baler shell from SU4, (F) eggshell (?) from SU3, (G) echinoderm, shell and coral fragments from SU4, (H) fossil shell within limestone from SU3 and (I) cross-section through echinoderm ossicle from SU5. (For interpretation of the references to colour in this figure legend, the reader is referred to the web version of this article.)

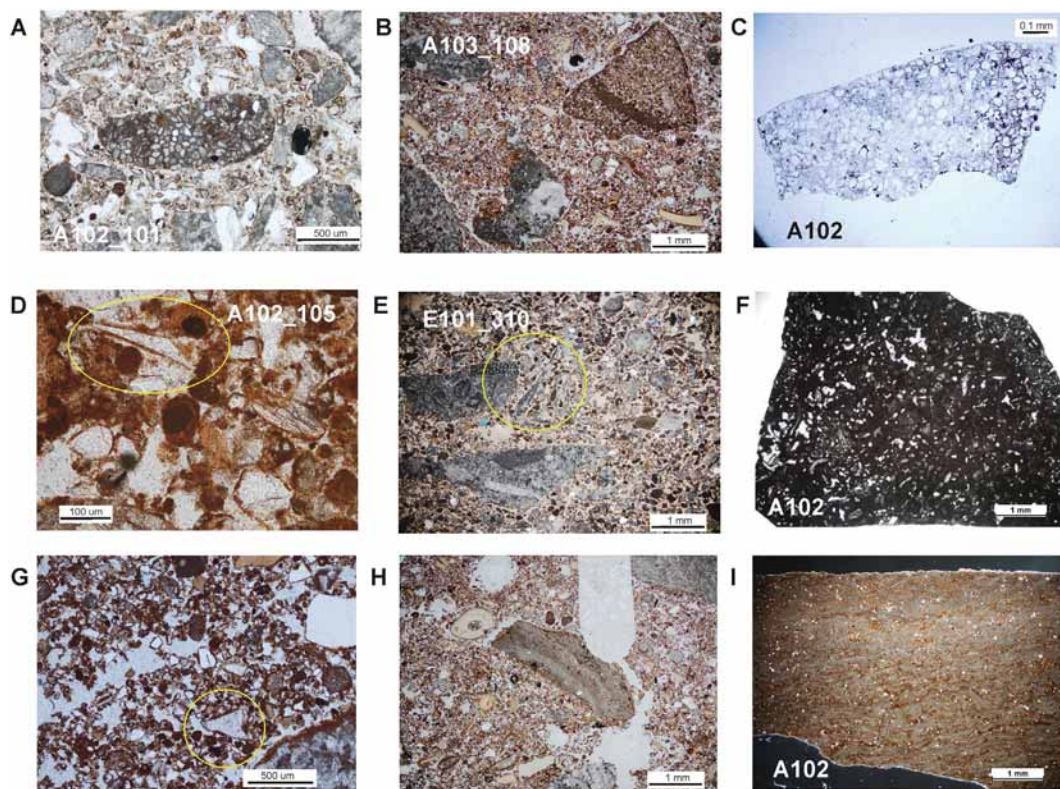


Fig. 16. Examples of lithic and related fragments from Boodie Cave, including (A) pelloid from SU2, (B) sandstone fragment from SU8, (C) thin section of identified sandstone flake from A102, (D) possible quartz shard within SU5, (E) possible limestone shard from SU4, (F) thin section of identified limestone flake from A102, (G) possible limestone shard from SU8, (H) calcrete fragment in SU8, and (I) thin section of quarried calcrete fragment from north of Barrow Is.

artefacts are made (e.g. Fig. 16F). This, along with limestone's brightness, makes it almost impossible to distinguish limestone artefacts from naturally occurring angular fragments of limestone here (sensu Garrison, 2003). An exception is calcrete which has a different (laminated) petrology to Trealla Limestone (Fig. 16I), so can be positively identified (e.g. Fig. 16H). Although they are rare in the stone artefact assemblage, the non-local materials such as sandstone (e.g. Fig. 16C), chert, igneous and metamorphic rocks should also be easier to identify by virtue of their exotic lithologies. However, even here, care has to be taken since some lithic materials can appear non-local but actually represent a natural material, such as pelloids that derive from shallow intertidal environments (e.g. Fig. 16A).

Despite these difficulties, differences noted in the angularity of grains along with comparisons between identified artefact thin sections from Boodie Cave has indicated some potential artefact fragments in the micromorphological thin sections. This includes a potential sandstone fragment (Fig. 16B), some particularly angular limestone fragments (Fig. 16E, G), an angular quartz shard (Fig. 16D) and one potential calcrete fragment (Fig. 16H). In contrast to other types of cultural materials, the observed stone artefacts are generally not weathered to any degree. Unfortunately these identifiable artefacts are too few in number to infer anything meaningful in terms of processes.

3.5. Post-depositional processes and taphonomy

Post-depositional processes within the cave sediments are mainly physicochemical and biological in origin. Detailed section drawings and photogrammetric renderings show small roots and insect burrows in the profile, which have left voids (e.g. Fig. 17L) and passage features (e.g. Fig. 9C and 17W). Micromorphological sections avoided these disturbed areas. The main post-depositional features within each stratigraphic unit are presented in Fig. 17, and summarised in Appendix Tables A3 and A4.

As may be expected, the oldest sediments displayed the greatest degree of post-depositional modification, including excrement fabrics (Fig. 17A), pellicular weathering (Class 2), and also iron-manganese hypocoatings and impregnative features (Fig. 17B), including around teeth (Fig. 13I) and bone (Table A3). A single concentric iron nodule around a limestone nucleus was observed at the base of SU9 (Fig. 17C) but is more likely to have been transported rather than formed in situ. In SU8, disaggregated crustal features (Fig. 17D) imply post-depositional disturbance of a formerly exposed surface, possibly by insects or other small creatures that resulted in the strong crumb microstructure and excremental products that are common at this level.

In SU7 and SU6, excremental products (Fig. 17E) start to become less common but pellicular weathering (Class 2) (Fig. 17F) is still evident. A relatively large (~2 cm) flattened and infilled plant/insect channel was observed in A106 (Fig. 9C). Iron-manganese impregnative features are also still evident, including around bone (Fig. 17G), along with a few orthic Fe/Mn nodules around a limestone or quartz nucleus (Fig. 17E). The latter imply periods of water saturation (Stoops et al., 2010), possibly favoured by the more damp conditions in these deeper sediments both in the past and in the present.

In SU5, iron nodules (Fig. 17I), manganese alteration products around a bone fragment (Fig. 17J) and pellicular alteration (Class 2) of limestone fragments (Fig. 17K), together imply a period(s) of alternating wetting and drying. Evidence of reworking is indicated from small extant root burrows and excremental fabrics (e.g. Fig. 17L). Contrasting this is the dense midden unit, SU4, as recorded at the front of the cave, which shows significantly less modification, no pellicular weathering of limestone, and only a few examples of Fe/Mn alteration of the bone (Fig. 17M) or nodule formation (Fig. 17N). This perhaps reflects the higher carbonate and lower terrestrial iron-oxide content of the sediments from which Fe/Mn-oxide alteration might occur but also likely drier conditions within these relatively porous sands. A single concentric iron nodule around a limestone nucleus (Fig. 17P) was

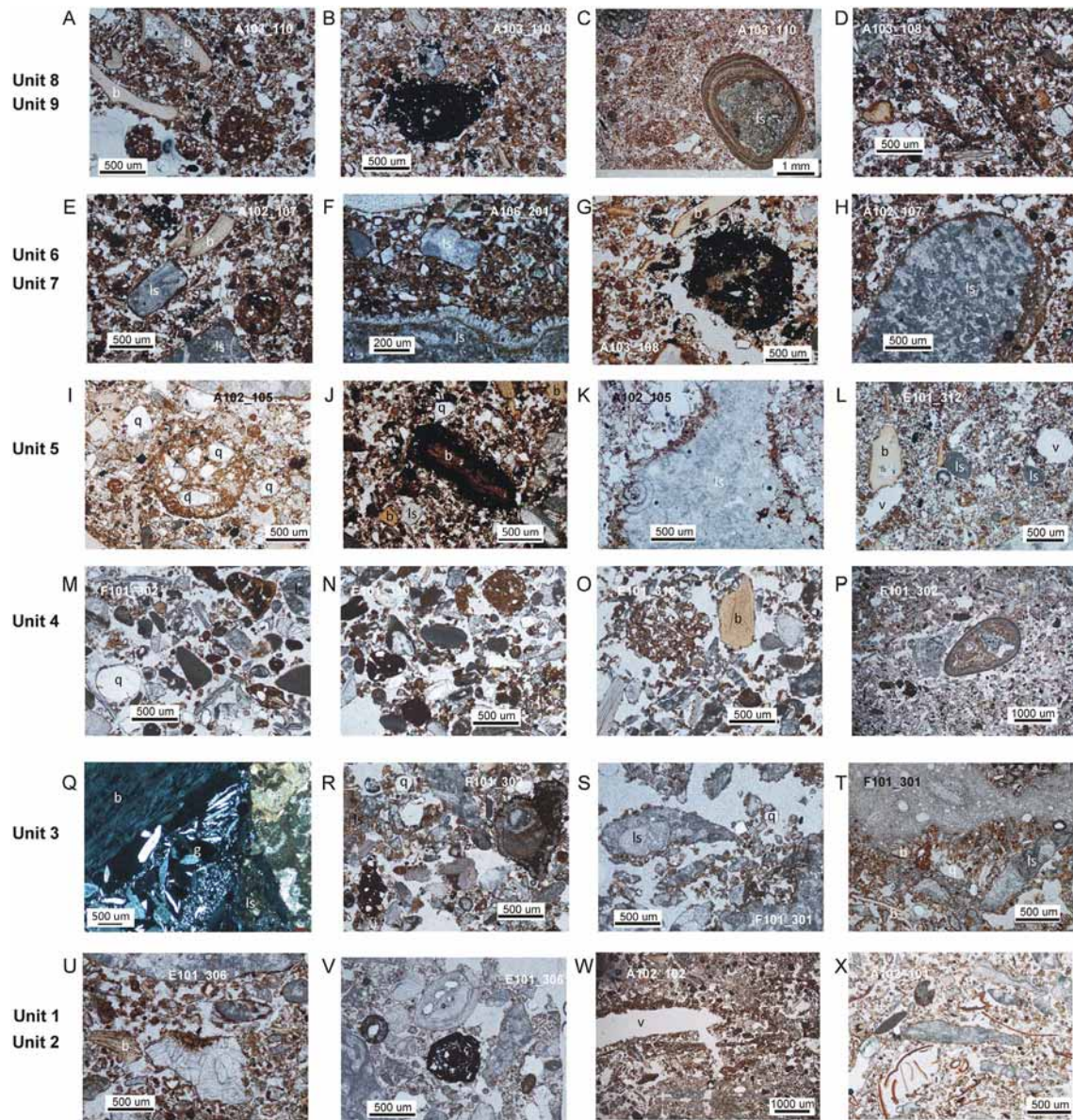


Fig. 17. Typical pedofeatures shown in each stratigraphic unit (in rows), including for: SU9 and SU8 (A) disaggregated crustal features, (B) moderate to strongly impregative manganese alteration, (C) excrement (spherical) fabric surrounding anorthic (?) concentric iron nodule with limestone (*ls*) nucleus, (D) disaggregated iron crusts; SU7 and SU6 (E) orthic nodules around quartz grains and iron-rich coatings around limestone (*ls*) and bone (*b*), (F) pellicular calcite alteration (Class 2) of limestone fragment, (G) typical Fe/Mn nodule within general excrement fabric, (H) pellicular iron alteration (Class 2) of limestone (*ls*) fragment; SU5 (I) orthic iron nodule around nucleus of quartz (*q*) grains, (J) manganese alteration around bone (*b*) fragment, (K) pellicular alteration (Class 2) of limestone fragment, (L) excrement (left) and calcite (right) around small round extant rootlet or burrow (*v*); SU4 (M) Fe/Mn alteration of bone (?), (N) typical Fe/Mn nodules, (O) orthic nodules, (P) anorthic (?) concentric iron nodule around limestone nucleus at SU3/SU4 interface; SU3 (Q) fibrous gypsum (*g*) intergrowths within void between bone and limestone fragment, (R) manganese alteration of bone and a strongly impregnated Fe/Mn nodule, (S) pellicular alteration (Classes 0–1) of limestone (*ls*) fragment, (T) carbonate re-cementing — present only in the front of the cave in square F101; and SU2 and SU1 (U) pellicular alteration (Classes 0–1) of limestone fragment, (V) concentric manganese nodule, (W) iron-rich silty quasiccoating around flattened plant/insect channel (*v*), (X) herbivore excrement (plant fibres).

observed at SU4/SU3 interface and is assumed from its form and isolated nature to be inherited rather than an *in situ* feature.

In SU3, particularly in the A102/A103 profile, gypsum intergrowths within void spaces are common (Fig. 17Q), corroborating what is observed in the field profiles. Iron and manganese alteration is present (Fig. 17R) but much less common, and pellicular alteration of limestone fragment is less acute (Class 0–1, Fig. 15S). In the front of the cave, in F101 only, carbonate re-cementing is evident in thin section (Fig. 17T) corroborating what was encountered in the field excavation. Above this, in SU2 and SU1, iron-manganese alteration (Fig. 17V) and pellicular alteration (Class 0–1) of limestone fragments becomes minimal or absent. A single iron-rich silty quasi-coating around a flattened plant/insect channel was observed in SU2 (Fig. 17W). There is also evidence

of relatively more recent disturbance in these upper units the form of herbivore excrement (plant fibres) (Fig. 17X).

Overall the micromorphology indicates pedological development is greatest within the oldest units, when it is assumed lower rates of discard and occupation facilitated preservation. In the middle units, as the use of the cave increased, pedological development decreases, with bioturbation and post-depositional modification generally constrained within one or two stratigraphic units (i.e. it is synsedimentary) rather than occurring between them. From micromorphological analyses the vertical zone within which material is being reworked is estimated to be between 1 and 5 cm, largely based on the subtle mineralogical and textural variations (microfacies) preserved within each unit. This reworking does not affect the general sequence of macro-cultural changes.

4. Discussion

Cave sites have complex depositional and post-depositional histories and require a detailed approach to understanding formation processes. As with other great caves including Die Kelders Cave (Goldberg, 2000), Blombos (Haaland et al., 2016), Vangard (Macphail et al., 2012), Niah Cave (Stephens et al., 2005, 2017) and Liang Bua (Morley et al., 2017), Boodie Cave greatly benefits from a multi-disciplinary approach anchored by contextual information from micromorphological analysis. The following discussion interprets the micromorphological evidence in relation to site formation and cave dynamics over its 50,000 years of occupation.

4.1. Cave sedimentary dynamics

Micromorphological investigations corroborate previous interpretations of the changing palaeoenvironmental context of Boodie Cave (Ward et al., 2017; Veth et al., 2017), as well as providing important new information regarding the occupation and formation history of the cave. The change from a polyminerologic quartz-rich assemblage to a simpler carbonate dominated assemblage from the terminal Pleistocene, reflects the cave's changing regional landscape context associated with post-glacial sea-level rise. However it is only once the sea is proximal that these changes become significant, with sediments reflecting a cave environment that is significantly buffered from larger-scale external changes.

The sedimentary record indicates that deposition occurred initially under relatively closed and moist cave conditions, with little external sediment input. The subsequent opening of the cave sometime around ~50 ka BP, allowed greater input of externally-derived sediments as reflected by the relatively high quartz, feldspar and heavy mineral component of the sediments, most likely deriving from reworked dune sands (see also Ward et al., 2017). The sharp boundary between SU9 and SU8 is indicative of an erosional surface and suggests that the opening of the cave may have been associated with flooding or some other high-energy event. Following this high-energy event, and during early cave occupation, depositional conditions were of comparatively lower energy, with an approximate sedimentation rate around 4 cm/ka. The presence of disaggregated crusts within SU8 indicates there was a period of stabilisation and exposure of the surface sediments (i.e. the existence of a temporal palaeosurface). The subsequent disturbance of this crust through bioturbation from insects or other burrowing organisms – evident from the excrement fabric and crumb microstructure – and local leaching of the sediments, implies that occupation or use of the cave at this time was of a low intensity. Evidence of occupation is implied from micro-fragments of charcoal, bone and shell and is supported by macro-scale evidence that shows remains of coastal species including mangrove gastropods (Veth et al., 2017).

In contrast, the following period represented by SU7 was one of increasing instability with significant rock fall particularly at the front of the cave opening up the cave to more exogenous sediments. These were most likely reworked dune sediments consistent with the unimodal iron-oxide-rich sands (see also Ward et al., 2017). Clay mica (illite) is a dominant clay mineral along with kaolinite in NW Australia, and is similarly indicative of low to moderate weathering in arid climatic conditions (Gingele et al., 2001). Sedimentation rate is almost double that of the previous period, at around 7 cm/ka. The subsequent period, represented inside the cave by SU6, likely represents one of infilling and levelling behind the front rockwall, allowing sediments from both exogenous and endogenous sources to accumulate across the whole of the front of the cave (at a net sedimentation of just under 4 cm/ka). It is at that stage that a lateral continuity is observed between the excavation profiles at the front and inside of the cave. The transition from unimodal dune sands to more multimodal sediments may indicate a period of vegetation growth at the front of the cave providing more sheltered conditions and localised weathering of sediments inside the

cave. This is the period when use of the cave starts to increase, with significantly higher percentages of bone apatite recorded in thin sections and macroscale evidence of arid zone fauna, and use of *Acacia* sp. and *Eucalyptus* sp. as fuel timbers (Veth et al., 2017).

Some parts of the cave however remain unstable. For example, the relatively homogenous sediments and mixed chronology in the upper A106 and A107 profile likely represents a slumping event. This localised event may have been favoured by a low point in the cave around the point of these excavation squares, as evidenced from the runoff and deposition of small amounts of fine sediment into the cave after Cylone Olwyn in 2015 (Fig. 3) and by an earlier in-wash event within SU7 in the A106 profile (Fig. 9C). A chronological discontinuity (sensu Veth et al., 2017) follows sometime after ~36 ka BP. A marked decrease in the coarse rubble (> 4 mm) fraction and increase in organic content (and hence colour) of the sediments, particularly at the front of the cave, implies increasing stability within the cave sedimentary system. There is otherwise no evidence for a change in sediment dynamics from the < 2 mm sediment fraction or mineral content at this transition. Nor is there any hiatus in the cultural records (see Veth et al., 2017). Hence this discontinuity is more accurately described as a diastem (low or zero net sedimentation). The average sedimentation rate for SU5 is estimated around 2.5 cm/ka. If sedimentation during the diastem is assumed to be a fifth of this level and the maximum zone of reworking is estimated at 5 cm or less, then this would equate with the 5–7 cm of sedimentary record that has subsequently become undifferentiated in the profile.

Unit 5 is a thick depositional sequence (20–40 cm), with micromorphological sampling only targeting the upper and lower boundaries. Cave use is clearly evident throughout the 15,000 years of sedimentation, with high abundances of burnt and unburnt faunal material, lithics and variably preserved charcoal (see also Veth et al., 2017), and indications of trampling from bone fragmentation within the sediment profile. Anthracological, zooarchaeological, malacological and micromorphological evidence all show that the heating of gathered food resources occurred at low temperatures, with large hearth features largely absent. Fuelwood was locally sourced, and included coastal trees such as wirewood (*Acacia coriacea*), wattle (*Acacia startii*), white mangrove (*Avicennia marina*) and ribbed mangrove (*Bruguiera exaristata*). The presence of mangrove species complement the results from grain size analyses and indicate that mangrove systems were likely established and easily utilized by past occupants around this time.

In the upper part of SU5, which is Holocene-aged, both the micromorphology and previous mineralogical analyses (Ward et al., 2017) show a marked increase in the exogenous biogenic carbonate content – including fragments of economic species – in association with Post-glacial sea-level rise. This culminates in Unit 4, the dense midden unit – or more accurately midden units, which show an abundance of highly fragmented utilitarian (*Melo* sp., *Tridachna* sp. and *Dentalium* sp.) and economic shell (echinoderm and gastropod), with associated exogenous biogenic sand from a proximal shallow-marine source, as implied from the fragmented and water worn shell remains. Studies elsewhere have indicated that such sands may have been introduced on animals, shellfish and seaweed gathered from the foreshore and/or introduced by feet and hands after harvesting (Fieller et al., 1984). Certainly there is micromorphological evidence of trampling, particularly in the upper part of this unit, hence some biogenic sand could have been transported this way. Alternative origins of the sands may include the creation of a clean firepit for cooking or even to put out a fire. Whatever the mode of deposition, the absence of discrete and dense midden unit(s) further inside the cave implies they were focused on the front of the cave, and were discarded over a short period, perhaps as little as 400 years.

Following midden accumulation, cave sediments are increasingly coarse-grained (> 2 mm) and dominated by exogenous biogenic (beach) sands most likely from proximal marine sources. This is arguably another period of instability in the cave as evident from significant

increase in the rubble component from the SU3/SU2 interface and an overall high net rate of sedimentation over 20 cm/ka. Despite evidence of bioturbation working across unit boundaries, zooarchaeological remains — which include articulated fish cranial elements, indicate a high degree of preservation aided by the high rate of sedimentation and higher carbonate content of the sediments but also possibly because the cave was abandoned. As outlined above, grain size samples in SU3 indicates sediments were likely reworked from one or more sources that may include mangrove environments. Anthracological analysis (A102/A103) show presence of two mangrove species, *Avicenna marina* (white mangrove) and *Bruguiera exaristata* (ribbed mangrove) within this unit. Whilst *Avicenna marina* grows in all tidal ranges, *Bruguiera exaristata* is generally found in the landward zone of mangrove communities, where it is inundated less frequently (Tomlinson, 1986). This suggests people were preferentially exploiting the more littoral parts. The dominance of *Terebralia* sp. in this midden layer would also support the mangrove environment as being highly important.

The topmost units, dated between 6.8 and 1.7 ka BP, cover the period of island abandonment (Veth et al., 2017). Sediments in these uppermost units are dominated by reworked carbonate sands from the now proximal coast, with lower rates of net sedimentation between 2 and 10 cm/ka and periods of depositional stability implied from the development of crustal boundary at least in some parts of the cave between SU2 and SU1. Overall pedogenic development within these uppermost sediments is low and may have aided preservation of archaeological remains in the underlying units. Micromorphological analyses indicate localised reworking with an average mixing zone between 1 and 5 cm, which predictably is greatest where net sedimentation is lowest. Grave and Kealhoefer (1999) similarly observed highly localised mixing from micromorphological and phytolith analysis, albeit with slightly lower scales of bioturbation (200–5000 µm). The key excavation squares dated within Boodie Cave have overall good stratigraphic integrity with a generally coherent sequence of macro-cultural and chronological changes, borne out by the clear changes in different assemblages of dietary fauna shifting synchronously with sediment sources, sea level fluctuations and occupation phase boundary dates derived from Bayesian modelling (Veth et al., 2017).

4.2. Comparisons of the sedimentary record inside with the front of the cave

Occupation and use of caves often occurs at the entrance, and bioturbation is also generally more intense close to the entrance (Karkanas and Goldberg, 2013). The high stratigraphic differentiation and archaeological preservation at the front of Boodie Cave compared to the deposit inside is thus unexpected. This may partly relate to the activities of the Burrowing bettong, which prefers the intermediate reaches of the cave and/or a relatively low level of human disturbance of the cave generally. Another factor may be the positioning of the excavation square away from what may have been the main entrance and/or area of use or occupation. Future excavations in Boodie Cave will target the talus slope in front of the cave as these seem to have surprisingly well preserved remains that may have been protected by now collapsed cave roof/driplines.

Microbats (*Vespadelus finlaysoni*) also inhabit the darker recesses of large and deep caves such as Boodie Cave. Gypsum, chitin fragments and decayed amorphous fine plant residues are associated with bat guano (Karkanas and Goldberg, 2013), however in Boodie Cave only chitin fragments are obvious and generally only within the surface sediments. As may be expected, chitinous fragments are marginally more abundant inside the cave than at the entrance. Where caves are poorly exposed to light, cryptomagic plants (algae, fungi, mosses) can predominate but tree and bush roots may occur as well (Karkanas and Goldberg, 2013). In Boodie Cave, modern *Ficus platypoda* tree roots are present at the front of the cave, where they penetrate about 2 m inside the cave, to depths of 80 cm or more. Inside the cave, finer rootlets are more common in the excavation profiles, occurring to depths of a

metre, but the majority of these are not considered to be extant (e.g. Fig. 17L). Some larger infilled hollows (e.g. Fig. 9C) and open cavities may indicate that larger rootlets once penetrated deeper into the cave, although these could equally have originated from burrowing organisms (e.g. lizards). Regardless, the conclusion is that reworking is greater inside the cave than at the entrance.

Where gypsum ($\text{CaSO}_4 \cdot 2\text{H}_2\text{O}$) is present, it tends to be more pervasive, concentrated between grain voids rather than as discrete crystals, particularly in Unit 3 in the A102/A103 excavation profile. Whilst the origin of this gypsum is pedogenic, its accumulation below the surface indicates it relates to an earlier wetter period (Poch et al., 2010), here dated to around the early Holocene. At this time, the transgressing coast may have increased the supply of sulphur from sea spray, which then seeped through the limestone ceiling and subsequently concentrated in the sediments through evaporation (Finlayson and Hamilton-Smith, 2003). Once proximal, the contemporary sea level and modern climatic conditions may have limited gypsum precipitation in the younger sediments and at the front of the cave due to the solubility of gypsum being raised in the presence of sodium chloride (Shaffer, 1967).

Deeper in the profile, another clear differentiation between the front and interior cave profiles can be seen in the predominance of carbonate-encrusted bone remains in the front excavation squares, particularly in SU5. In alkaline settings, objects are typically encrusted with carbonate because of presence of carbonic acid (H_2CO_3) that causes carbonate (including limestone) features to dissolve. Rainwater is slightly acid (~pH 5.6). As the front of the cave is more exposed to rain-splash and runoff, carbonate dissolution is more likely to occur there. The preferential encrustation of bone over other cave materials may relate to its microcrystalline nature (hydroxylapatite) that makes it more susceptible to changes in soil moisture and/or alkalinity (Berna et al., 2003).

Both the sediments and the material remains inside caves may differ from open-air or above ground sites (Ward et al., 2006), the latter which reflect a high-proportion of exotic lithologies from the mainland (Veth et al., 2014, 2017). The distinction between interior and exterior space is also reflected in the concentration of artefacts and middens in the lighter zones compared to deeper parts of the cave, but also importantly in the variable nature of bioturbation and geochemical processes. Such variation is likely to change as the morphology of the cave and cultural use of the cave space varies over time.

5. Conclusion

As in other cave sites, the micromorphological investigation of Boodie Cave helps address key questions relating to reliability of inferred relationships between finds and within deposits, the nature and duration of natural events and processes (such as roof-fall, runoff, post-depositional bioturbation), the influence of human activity on local sedimentary and pedological processes, and the extent to which the cave environment is buffered from external larger-scale changes until a certain threshold — or sea level, is reached. The addition of automated mineralogical analysis (QEMSCAN® or TIMA®) provides a complementary empirical and visual analysis of sediment composition that can enhance interpretations made from thin section.

Interpretations of the dynamics and stability of Boodie Cave and its wider landscape context are clearly influenced by the spatio-temporal scale at which it is observed. At the micro-scale there is evidence of minor post-depositional modification and intra-strata mixing to depths between 1 and 5 cm, and is greater inside the cave than at the entrance. This mixing has not significantly compromised the macro-cultural trends and provides acceptable confidence levels for the generally high integrity of the archaeological deposits. At the macro-scale level, there is little inter-strata mixing within the cave sediments, with the exception of A106 and A107, where perturbations in the upper units hint at larger landscape processes. Coarse differentiation of strata and higher

energy deposition and rock-fall events can be observed in the coarse (> 2 and > 4 mm) sediment fractions. With each new strata, depositional disturbances – both natural and cultural – are incorporated and a sedimentary homeorhesis is established within the cave.

Taken at a landscape level, the cave and the human use of it absorbed a range of perturbations and climatic variations, including the extreme aridity of the LGM and frequent monsoonal cyclones. Initially humans have been responsible for punctuated and likely short-lived impacts on the formation history of Boodie Cave, with evidence for early occupation and coastal reliance within the Australian context. Later, in the Holocene, increased human activity is evident from exogenous biogenic sands and cultural debris within the cave, which reduced the level of pedogenic development within the sediment profile. It is only once the island was cut off from the mainland that human resilience is ultimately challenged, leading to its apparently rapid abandonment after 7 ka.

Acknowledgements

The Barrow Island Archaeology Project (BIAP) was funded by an Australian Research Council Discovery Project (DP130100802) awarded to PV, TM, Alistair Paterson, MB, DZ, CP and Corioli Souter, and administered by the University of Western Australia. Research Associates include PK, IW and FH. TM is supported by Australian Research Council DECRA Fellowships (DE150101597). Department of

Parks and Wildlife, Archaeaus, Chevron Australian Business Unit and WA Oil are thanked for their logistical and personnel support both in the planning process and in the field. Emilie Dotte-Sarout, Sean Winter and IW managed the project and Bob Sheppard managed health, environmental safety and quarantine planning and the construction and operation of the field camp. Russell Lagdon and Kris Holmes are thanked for their detailed advice and support for the Barrow Island fieldwork. Funding for UT was obtained by Penelope L King (DP150104604). The authors acknowledge the facilities, and the scientific and technical assistance, of the Australian Microscopy and Microanalysis Research Facility at the Centre for Advanced Microscopy (CAM), Australian National University, Canberra. In particular, we thank Frank Brink from CAM for help with QEMSCAN® analyses. We acknowledge the participation and support of Buurabalayji Thalanyji Aboriginal Corporation and Kuruma Marthudunera Aboriginal Corporation.

IW conducted geoarchaeological investigations, including stratigraphy and micromorphology, and wrote the text with specialist contributions from other authors. LP, TD and UT provided QEMSCAN® and QXRD analyses. KD provided analyses on stone artefacts, TM analysed the vertebrate assemblage, CB analysed the archaeobotanical assemblages, and FH analysed the marine invertebrate assemblage. PK provided samples from Ledge Cave and background information on Barrow Island. We wish also to acknowledge the two anonymous reviewers for their helpful comments on the manuscript.

Appendix A

Table A1

Summary table of micromorphology inside Boodie Cave (from A102/103 and A106/107).

	SU	Microfacies	Slide no.	Chronology (ky BP)	Macrostratigraphy	Micromorphological description	Microstructure/groundmass	Pedofeatures
Holocene	1	A	101	< 1.7	Unconsolidated, poorly sorted, coarse-med, red-brown (2.5YR 5/8) silty sands with abundant angular pebbles	Sub-angular limestone fragments (50%), burnt and unburnt bone (10%) and shell (5%) fragments, quartz (f.s.–m.s. 5–10%). Porosity ~ 5%.	Complex (intergrain) microstructure (c/f ratio 70:30), grading to compact (equal enaulic) microgranular fabric.	Disaggregated dung (plant and chiton) (5%)
		B	101	< 1.7	As above	Compacted limestone, quartz (f.s.–m.s. 5–10%).	Compact (equal enaulic) microgranular fabric at unit boundary.	
	2	A	102, 103	2.5–6.8	As for 1 but slightly darker (2.5YR 4/6) silty sands	Sub-angular limestone fragments (25%). Decreased bone (inc. fewer burnt) fragments (5%), shell (2%), quartz (f.s. 5%)	Open enaulic microgranular structure (c/f ratio 40:60). Calcitic crystallitic b-fabric. Inter-aggregate porosity 20%.	Iron oxide impregnative coatings and hypocoatings around grains, and occasionally concentrated around voids
3	B						Localised concentration of iron	
	A		103	6.8–7.2	Darker red-brown (7.5YR 4/6), moderately sorted, medium-fine sands with abundant semi-rounded pebbles and finely disseminated charcoal	Angular to sub-angular limestone (c.s. > 50%) with sub-rounded to well-rounded quartz (f.s.–c.s. 5%). Increased bone content (20%), minor shell (5–10%).	Moderately birefringent (limestone silt) groundmass, with speckled b-fabric (c/f ratio 80:20). Not compacted enaulic distribution. Inter-aggregate porosity 30%.	Lenticular gypsum (m.s.–c.s.) infilling pore spaces (up to 20%), locally intergrown, forming massive aggregates, also in groundmass (5–10%)
Pleistocene	5	A	104–106, 201	7.2–18	Moderately compacted, poorly sorted, dark red (2.5YR 3/6) medium-fine sands with abundant pebble-sized limestone fragments (roof fall)	Angular to sub-angular limestone (c.s.) with sub-rounded to well-rounded quartz (f.s.–c.s. 10%), feldspars (< 5%). Bone (20–40%), including some burnt (2%), shell (1%) and plant fragments (8–10%).	Compacted enaulic to porphyritic distribution (c/f ratio 30:70). Increased quartz (f.s.–m.s.) (20% groundmass). Calcitic crystallitic b-fabric. Inter-aggregate porosity < 20%.	Occasional infilled plant/insect burrows (1–2 mm diameter). Impregnative Fe- and irregular Mn-oxide pedofeatures. Carbonate dissolution (pellicular weathering — Class 1) around limestone fragments.
		B			As above	As above	As above	As above with few infilled burrows. Localised concentration of iron-stained minerals
6	A		107, 202	29–42	Moderately sorted coarse calcitic sand, with degraded angular limestone clasts (20%) and significantly increased bone content (< 50%)	Angular to sub-rounded limestone fragments (10%), feldspars (< 5%). Bone (15–20%), shell (2%), plant fragments (8–10%).	Compacted enaulic to porphyritic distribution (c/f ratio 40:60), increased quartz (f.s.–m.s.) (< 40% groundmass). Inter-aggregate porosity 10%.	Increased Fe-oxide impregnative coatings and hypocoatings around grains. Calcitic hypocoating around some bone fragments. Single loose infilled oval plant/insect burrow (0.5 × 1 cm).
		A	108, 203	42–48	Well-compacted, moderately sorted, med-fine iron-stained calcitic sand with fewer large clasts and increasing quartz (5–10%), few feldspar and	Sub-rounded limestone fragments (10%), quartz (f.s.–c.s. 10%), feldspar (5%) and tourmaline grains (1%). Increased bone (20%), shell (2%), plant	Fine enaulic grading into porphyritic (c/f ratio: 40: 60). Increased quartz (f.s.–m.s.) (< 50% groundmass). Calcitic crystallitic b-fabric. Inter-	Abundant Fe- and Mn-oxide pedofeatures of various morphologies.

8	A	109, 110	48–53	heavy minerals (tourmaline) (1%) Well-compacted, moderately sorted dark red (2.5YR 3/6) silty sand with increasing cobbles (roof fall?) Similar to 6 but slightly lighter (2.5YR 5/8 grading to 5YR 6/8), with pebble lens in West wall	fragments (4–6). Few large angular to sub-limestone fragments (20%), quartz (f.s.–m.s. 20%), feldspar (5%) and tourmaline (< 1%). Bone (10–20%), eggshell (< 1%), plant fragments (2–4). One or more quartz (f.s.) lenses a few grains thick in 203.	aggregate porosity < 20%. Open enaulic to granular microfabric (c/f ratio 80:20). Quartz (f.s.–m.s.) (~50% groundmass). Calcitic crystallitic b-fabric. Inter-aggregate porosity 40%.	Abundant Fe- and Mn-oxide pedofeatures. Single infilled longitudinal plant/insect burrow (width 3 mm).
9	A	110	~77	Darker red-brown, moderately sorted clayey sand with discrete (?) pebble lens at base of Nth Wall	Few large angular to sub-limestone fragments (10%), quartz (f.s.–m.s. 30%), feldspar (5%). Decreased bone (5–10%).	Compact (equal enaulic) microgranular structure. Quartz (f.s.–m.s.) (~50% groundmass). Calcitic crystallitic b-fabric. Inter-aggregate porosity 10%.	Fe- and Mn-oxide pedofeatures, with single concentric Fe-nodule around limestone. Carbonate dissolution (pellicular weathering — Class I)

Table A2

Summary table of micromorphology at the front of Boodie Cave.

SU		Microfacies	Slide no.	Chronology (ky BP)	Macrostratigraphy	Micromorphological description	Microstructure/groundmass	Pedofeatures
Holocene	1	1A	306	2.5–1.7	Moderately compacted, poorly sorted, pale red (2.5YR 5/8) shelly-silty sand with shell flakes (3–4 mm) packed and oriented horizontally	Sub-angular limestone fragments (50%), burnt and unburnt bone (10%) and biogenic shell (5%), quartz (f.s.–m.s. 5–10%). Porosity ~5%.	Complex (intergrain) microstructure (c/f ratio 60:40), grading to compact (equal enaulic) microgranular fabric at unit boundary.	Disaggregated dung (plant and chiton) (5%). Iron oxide impregnate coating around grains.
	2	2A	307	6.8–2.5	As above but slightly paler (2.5YR 6/6)	Sub-angular limestone fragments (40%). Decreased bone (inc. fewer burnt) fragments (5%), biogenic and other (baler) shell (2%), quartz (f.s. 5%)	Open enaulic microgranular structure (c/f ratio 40:60). Calcitic crystallitic b-fabric. Inter-aggregate porosity 15%.	Iron oxide impregnate coatings and hypocoatings around grains, and occasionally concentrated around voids
		2B	308		Increasingly compacted, moderately sorted, light reddish brown (5YR 6/3) carbonate-rich sandy silt, with < 10% flaked shell fragments and large pebbles	As above with slightly lower abundance of coarse limestone (30%).	As above	As above
	3	3A	301/ 309	7.4–6.8	Darker red-brown (7.5YR 4/6), moderate to poorly sorted, medium-fine sands with abundant angular limestone fragments	Angular to sub-angular limestone (c.s. > 50%) with sub-rounded to well-rounded quartz (f.s.–c.s. 5%), minor feldspar (2%). Increased bone content (20%), minor shell (5–10%).	Moderately birefringent (limestone silt) groundmass, with speckled b-fabric (c/f ratio 70:30). Not compacted enaulic distribution. Inter-aggregate porosity 20%.	Iron oxide impregnate coatings and hypocoatings around grains. Carbonate cementing in F101
		3B	301/		As above	As above	As above	Slightly more iron oxide

Table A3
Frequency of microfutures and post-depositional alteration features inside Boodie Cave.

Sample info	Lithofacies	Slide no.	Frequency			Bioturbation & excrement				Translocation & concentration				Clast alteration		Bone alteration		Plant pseudomorphs
			Micro-bones	Charcoal	Malacofauna	Egg-shell	Burrow mould	Excrement	Silt/clay capping	Fe/Mn nodule	Other Fe/Mn	Gypsum void/growth	Pellicular calcite	Secondary calcite	Unburnt: burnt	Mn coat		
1	A	101	Very few	Few	Few (biogenic)	None	None	Few	Very few	None	Very few	None	None	None	1:10	Zero	Zero	
2	B	101	Very few	Zero	Very few	None	None	None	Very few	None	Very few	None	None	None	0:10	Zero	Zero	
	A	102, 103	Very few	Zero	Few (biogenic)	Very few	Very few	Very few	Very few	None	Very few	Few	Very few	None	2:10	Very few	Zero	
	B		Few	Zero	Common	Very few	None	Very few	Very few	None	Few	Common	None	None	2:10	Very few	Zero	
3	A	103	Common	Zero	Common	Very few	None	Few	Few	None	Very few	Common	None	None	1:10	Few	Few	
5	A	104–106, 201	Frequent	Few	Very few (biogenic)	Few	Very few	Common	Common	None	Few	Common	Few	Common	5:10	Few	Very few	
	B		Frequent	Few	Few (baler)	Few	Very few	Common	Common	None	Few	Few	Common	Few	5:10	Few	Few	
	C		Frequent	Few	Few (baler)	Very few	Very few	Common	Common	None	Very few	Very few	Common	Very few	5:10	Few	Few	
6	A	107, 202	Common	Zero	Very few	Very few	None	Few	Common	None	Very few	None	Common	Very few	4:10	Very few	Very few	
7	A	108, 203	Few	Zero	Few (baler/other)	Very few	None	Frequent	Frequent	None	Few	None	Common	None	2:10	Very few	Very few	
8	A	109, 110	Few	Very few	Very few	Few	None	Frequent	Frequent	None	Few	None	Common	None	0:10	Few	Very few	
	B		Common	Very few	Very few	Few	None	Frequent	Frequent	None	Few	None	Common	None	0:10	Common	Very few	
9	A	110	Few	Zero	Very few	None	None	Common	Frequent	Very few	Few	None	Common	None	0:10	Few	Very few	

Table A4
Frequency of microfutures and post-depositional alteration features at the front of Boodie Cave.

Sample info	Lithofacies	Slide no.	Frequency			Bioturbation & excrement				Translocation & concentration				Clast alteration		Bone alteration		Plant pseudomorphs
			Microbones	Charcoal	Malacofauna	Eggshell	Burrow mould	Excrement	Silt/clay capping	Fe/Mn nodule	Other Fe/Mn	Gypsum void/growth	Pellicular calcite	Secondary calcite	Unburnt: burnt	Mn coat		
1	A	306	Very few	None	Very few	None	None	Few	Very few	None	Very few	None	Very few	None	0:10	None	Very few	
2	A	307	Very few	None	Very few (biogenic)	None	Very few	Few	Very few	None	Very few	None	Very few	None	1:10	None	None	
	B	308	Very few	None	Few (inc. baler)	Very few	None	Very few	Very few	None	Very few	None	Very few	None	1:10	None	Very few	
3	A	301/309	Very few	None	Few	Very few	None	Very few	Few	None	Very few	None	Few	None	1:10	Very few	None	
	B	301/309	Very few	None	Few (biogenic)	None	None	Very few	Few	Very few	Very few	None	Few*	Cementing	1:10	Very few	None	

4	A	302/ 303/ 310	Few	None	Very few	None	Very few	None	Very few	2:10	Very few	None	Very few
	B	302/ 303/ 310	Few	None	Very few	None	None	None	Very few	1:10	None	Very few	None
	C	302/ 303/ 311	Few	None	Very few	None	None	None	Very few	1:10	None	None	None
5A	A	304/ 311	Few	Very few	Few	Few	Few	Few	Few	3:10	Very few	Very few	Few
	B	305	Common	Very few	Few	Few	Common	Common	Common	4:10	Few	Few	Few
	C	312	Common	Very few	Few	Common	Common	Common	Common	1:10	None	None	Very few
6	A	312	Few	None	Very few	None	Common	Few	Common	0:10	None	None	Very few
7	nd	nd	Few	None	Very few	None	Common	Few	Common				

References

Berna, F., Mathews, A., Weiner, S., 2003. Solubilities of bone mineral from archaeological sites: the recrystallization window. *J. Archaeol. Sci.* 31, 867–882.

Butcher, A.R., Helms, T.A., Gottlieb, P., Bateman, R., Ellis, S., Johnson, N.W., 2000. Advances in the quantification of gold deportment by QEMSCAN. In: Alexander, D., Atasoy, Y., Browner, R., Cloutt, B., Dunne, R., Franzidis, J.P., Hewlett, D., Ibana, D., Nelson, M., Yan, D. (Eds.), Conference Volume: Seventh Mill Operators Conference, Kalgoorlie, W.A. 12–14 October Vol. 2000. The Australasian Institute of Mining and Metallurgy, Melbourne, Victoria, pp. 267–271.

Chevron Australia, 2014. Gorgon Gas Development and Jansz Feed Gas Pipeline. Terrestrial and Subterranean Baseline State and Environmental Impact Report. Available at: <https://www.chevronaustralia.com/docs/default-source/default-document-library/gorgon-emp-terrestrial-and-subterranean-baseline-state-and-environmental-impact-report.pdf> (accessed 06.04.17).

Courty, M.-A., Goldberg, P., MacPhail, R.I., 1989. Soils and Micromorphology in Archaeology. Cambridge Manuals in Archaeology. Cambridge University Press, Cambridge.

Department of Environment and Conservation (DEC), 2007. Management Plan for the Montebello/Barrow Islands Marine Conservation Reserves 2007–2017. Management Plan No. 55. Available at: https://www.dpaw.wa.gov.au/images/documents/parks/management-plans/decarchive/montebello-barrow-mp_final.pdf.

Edwards, T., Grono, E., Herries, A.I.R., Brink, F.J., Troitzsch, U., Senden, T., Turner, M., Barron, A., Prossor, L., Denham, T., 2017. Visualising scales of process: multi-scalar geoarchaeological investigations of microstratigraphy and diagenesis at hominin bearing sites in South African karst. *J. Archaeol. Sci.* 83, 1–11.

Faure, H., Walter, R.C., Grant, D.R., 2002. The coastal oasis: ice age springs on emerged continental shelves. *Glob. Planet. Chang.* 33 (1), 47–56.

Fieller, N.R.J., Gilbertson, D.D., Olbricht, W., 1984. A new method for environmental analysis of particle size distribution data from shoreline sediments. *Nature* 311, 648–651.

Finlayson, B., Hamilton-Smith, E., 2003. *Beneath the Surface: A Natural History of Australian Caves*. UNSW Press, Sydney.

Garrison, E., 2003. *Techniques in Archaeological Geology*. Springer.

Gingele, F.X., DeDeckker, P., Hillenbrand, C.-D., 2001. Clay mineral distribution in surface sediments between Indonesia and NW Australia — source and transport by ocean currents. *Mar. Geol.* 179, 135–146.

Goldberg, P., 2000. Micromorphology and site formation at Die Kelders Cave I, South Africa. *J. Hum. Evol.* 38 (1), 43–90.

Goldberg, P., Aldeias, V., 2016. Why does (archaeological) micromorphology have such little traction in (geo)archaeology. *Archaeol. Anthropol. Sci.* <http://dx.doi.org/10.1007/s12520-016-0353-9>.

Grave, P., Kealhoefer, L., 1999. Assessing bioturbation in archaeological sediments using soil morphology and phytolith analysis. *J. Archaeol. Sci.* 26, 1239–1248.

Haaland, M.M., Miller, C., Henshilwood, C.S., 2016. Geoarchaeological and micro-morphological investigations of Blombos Cave, South Africa. In: Society of Africanist Archaeologists 23rd Biennial meeting, Toulouse, France.

Haberlah, D., Strong, C., Pirrie, D., Rollinson, G.K., Gottlieb, P., Botha, P.P.W.S.K., Butcher, A.R., 2011. Automated petrography applications in Quaternary Science. *Quat. Australasia* 28 (2), 3–12.

Hickman, A. H., Strong, C. A. (2003). Dampier Barrow Island: 1:250,000 Sheet, Western Australia. Geological Survey of Western Australia, Perth.

Jankowski, N.R., Jacobs, Z., Goldberg, P., 2015. Optical dating and soil micromorphology at MacCauley's Beach, New South Wales, Australia. *Earth Surf. Process. Landf.* 40 (2), 229–242.

Karkanas, P., Goldberg, P., 2013. Micromorphology of cave sediments. In: Shroder, J., Frumkin, A. (Eds.), *Treatise on Geomorphology. Karst Geomorphology* Vol. 6. Academic Press, San Diego, pp. 286–296.

Macphail, R.I., Goldberg, P., Barton, R.N.E., 2012. Vanguard Cave sediments and soil micromorphology. In: Barton, R.N.E., Stringer, C.B., Finlayson, J.C. (Eds.), *Neanderthals in Context: A Report of the 1995–1998 Excavations at Gorham's and Vanguard Caves, Gibraltar*. Oxford University School of Archaeology, Oxford, pp. 193–210.

Mallou, C., Mentzer, S.M., 2015. Contacts under the lens: perspectives on the role of microstratigraphy in archaeological research. *Archaeol. Anthropol. Sci.* <http://dx.doi.org/10.1007/s12520-015-0288-6>.

Manne, T., Veth, P.M., 2015. Late Pleistocene and early Holocene exploitation of estuarine communities in northwestern Australia. *Quat. Int.* 385, 112–123.

Manne, T., Veth, P., Ward, I., Ditchfield, K., Hook, F., Dortch, J., Basgall, M., Zeanah, D., Skippington, J., Byrne, C., 2017. Pleistocene and early Holocene archaeological record of Barrow Island, northwestern Australia: early and sustained evidence for mixed use of coastal and arid interior settings. *Paleoanthropology Society 2017 Meeting Vancouver, Canada*.

Mentzer, S.M., 2014. *Microarchaeological Approaches to the Identification and Interpretation of Combustion Features in Prehistoric Archaeological Sites*. *J. Archaeol. Method Theory* 21, 616–668.

Moore, D., Reynolds, R.C., 1997. *X-ray Diffraction and the Identification and Analysis of Clay Minerals*, Second ed. Oxford University Press, New York.

Morley, M.W., Goldberg, P., Sutikna, T., Tocheri, M.W., Prinsloo, L.C., Jatmiko, E., Saptomo, W., Wasisto, S., Roberts, R.G., 2017. Initial micromorphological results from Liang Bua, Flores (Indonesia): site formation processes and hominin activities at the type locality of *Homo floresiensis*. *J. Archaeol. Sci.* 77, 125–142.

Moro, D., Lagdon, R., 2013. History and environment of Barrow Island. In: *Records of the Western Australian Museum*. 83. pp. 1–8 (Suppl.).

Ostrom, M.E., 1961. Separation of clay minerals from carbonate rocks by using acid. *J.*

- Sedim. Petrol. 31, 123–125. <http://dx.doi.org/10.1306/74D70B1E-2B21-11D7-8648000102C1865D>.
- Pirrie, D., Butcher, A.R., Power, M.R., Gottlieb, P., Miller, G.L., 2004. Rapid quantitative mineral and phase analysis using automated scanning electron microscopy (QemSCAN); potential applications in forensic geoscience. *Geol. Soc. Lond. Spec. Publ.* 232, 123–136. <http://dx.doi.org/10.1144/GSL.SP.2004.232.01.12>.
- Playford, P.E., 2014. Recent mega-tsunamis in the Shark Bay, Pilbara, and Kimberley areas of Western Australia. *J. R. Soc. West. Aust.* 97, 173.
- Poch, M., Artieda, O., Herrero, J., Lebedeva-Verba, M., 2010. Gypsic Features. In: Stoops, G., Marcelino, V., Mees, F. (Eds.), *Interpretation of Micromorphological Features of Soils and Regoliths*. Elsevier, Amsterdam, The Netherlands.
- Powell, E.N., Staff, G.M., Callender, R.W., Shton-Alcox, K.A., Brett, C.E., Parsons-Hubbard, K.M., Walker, S.E., Raymond, A., 2011. Taphonomic degradation of molluscan remains during thirteen years on the continental shelf and slope of the northwestern Gulf of Mexico. *Palaeogeogr. Palaeoclimatol. Palaeoecol.* 312, 209–232.
- Shaffer, L.H., 1967. Solubility of gypsum in sea water and sea water concentrates at temperatures from ambient to 65 degree. *J. Chem. Eng. Data* 12 (2), 183–189.
- Stephens, M., Rose, J., Gilbertson, D., Canti, M.G., 2005. Micromorphology of cave sediments in the humid tropics: Niah Cave, Sarawak. *Asian Perspect.* 44 (1), 42–55.
- Stephens, M., Rose, J., Gilbertson, D.D., 2017. Post-depositional alteration of humid tropical cave sediments: micromorphological research in the Great Cave of Niah, Sarawak, Borneo. *J. Archaeol. Sci.* 77, 109–124.
- Stoops, G., 2003. *Guidelines for Analysis and Description of Soil and Regolith Thin Sections*. Madison, Wisconsin.
- Stoops, G., Marcelino, V., Mees, F., 2010. Micromorphological features and their relation to processes and classification: general guidelines and keys. In: Stoops, G., Marcelino, V., Mees, F. (Eds.), *Interpretation of Micromorphological Features of Soils and Regoliths*. 2. Elsevier, Amsterdam, pp. 15–35.
- Tomlinson, P.B., 1986. *The Botany of Mangroves*. Cambridge University Press, Sydney.
- Vanniewenhuysse, D., O'Connor, S., Balme, J., 2017. Settling in Sahul: investigating environmental and human history interactions through micromorphological analyses in tropical semi-arid north-west Australia. *J. Archaeol. Sci.* 77, 172–193.
- Veth, P., Ditchfield, K., Hook, F., 2014. Maritime deserts of the Australian northwest. *Aust. Archaeol.* 79, 156–166.
- Veth, P., Ward, I., Manne, T., Ulm, S., Ditchfield, K., Dortch, J., Hook, F., Petchey, F., Hogg, A., Questiaux, D., Demuro, M., Arnold, L., Spooner, N., Levchenko, V., Skippington, S., Byrne, C., Basgall, M., Zeanah, D., Belton, D., Helmholz, P., Bajkan, S., Bailey, R., Placzek, C., Kendrick, P., 2017. Early human occupation of a maritime desert, Barrow Island, North-West Australia. *Quat. Sci. Rev.* 168, 19–29.
- Ward, I.A.K., Fullagar, R.L.K., Boer-Mah, T., Head, L.M., Tacon, P.S.C., Mulvaney, K., 2006. Comparison of sedimentation and occupation histories inside and outside rock shelters, Keep-River region, northwestern Australia. *Geoarchaeology* 21, 1–27.
- Ward, I., Larcombe, P., Mulvaney, K., Fandry, C., 2013. The potential for discovery of new submerged archaeological sites near the Dampier Archipelago, Western Australia. *Quat. Int.* 308–309, 216–229.
- Ward, I., Larcombe, P., Veth, P., 2015. A new model for coastal resource productivity and sea level change: the role of physical sedimentary processes in assessing the archaeological potential of submerged landscapes from the northwest Australian coastline. *Geoarchaeology* 30, 19–31.
- Ward, I., Merigot, K., McInnes, K., 2017. Application of quantitative mineralogical analysis in archaeological micromorphology: a case study from Barrow Is., Western Australia. *J. Archaeol. Method Theory*. <http://dx.doi.org/10.1007/s10816-017-9330-6>.